Chapter 11
Electromagnetic Effects Resulted from Explosions

Abstract In this chapter we study man-made low-frequency electromagnetic fields resulted from high explosive or nuclear detonations. The main emphasis is on underground explosion effects and a variety of accompanying electromagnetic phenomena caused by rock deformation and perturbations of the Earth magnetic field. We start with basic mechanisms for a so-called electromagnetic pulse (EMP) occurring just after the detonation and belonging to ULF/ELF frequency range. It is usually the case that the EMP precedes the co-seismic phenomena caused by seismic wave arrival at the observation point. Then we examine the atmospheric effects caused by the generation of dusty clouds and propagation of aerial shock waves (SWs). In the remainder of this chapter we consider the perturbations of the ionospheric plasma caused by an upward propagating SW.

Keywords Aerial shock wave (SW) • Electromagnetic pulse (EMP) • Gas-dust cloud • Residual electromagnetic field • Underground explosion

11.1 Diamagnetic Plasma Effect of Explosions

11.1.1 Observations of EMP Resulted from Underground Explosions

The earliest detailed recordings of the EMP caused by underground tests have been published after the series of nuclear detonations referred as Hardtack II on the proving ground in Nevada in 1958 (Zablocki 1966). At first the examination of ground conductivity was planned in the vicinity of an underground explosion chamber. However the strong low-frequency electric field was unexpectedly detected at the moment of detonation. The electric pickup arising simultaneously with the detonation was so high that it prevented seriously the recording of conductivity changes. These findings lent impetus to a study of interrelationship between electromagnetic and seismic effects because of importance of this research for the

V. Surkov and M. Hayakawa, *Ultra and Extremely Low Frequency Electromagnetic Fields*, Springer Geophysics, DOI 10.1007/978-4-431-54367-1_11,

treaty verification of nuclear undearground tests (e.g., Latter et al. 1961b; Gorbachev et al. 1999a,b). Much emphasis has been put on studies of the EMP in order to detect any underground nuclear testing especially in the case of the so-called decoupling of underground nuclear explosion (Zablocki 1966; Sweeney 1989). The decoupling means that the underground explosion is realized in an evacuated volume in the chamber of large size in order to diminish seismic effect of the explosion (Latter et al. 1961a; Herbst et al. 1961; Patterson 1966). Although the EMP magnitude of the explosion with decoupling can even be greater in comparison with that of the explosion conducting under the usual size of the explosion chamber (Gorbachev and Semenova 2000a,b).

Below we review experimental data and then focus on basic physical mechanisms of this phenomenon and estimate the amplitude of ULF electromagnetic variations. The observations have shown that the EMP of underground explosions decreases rapidly with distance so that it is practically undetectable at the distance over 10 km from the detonation point. For instance, the electric field amplitude was approximately 1 μV/m at the epicentral distance of 6.72 km (Zablocki 1966). A typical scheme of the recording electrodes arrangement under Hardtack II series of nuclear testing is shown in Fig. 11.1. The non-screened isolated copper wire with length of 750 m was laid on the ground from the observation point towards to the explosion epicenter in the East–West direction. The wire ends were linked with the lead electrodes buried in the ground 1–3 m deep. The same length wire was laid in the perpendicular North–South direction. Next one was put into a hole at the depth of 30 m. This wire is ended by the lead electrode as well. The recording sensors measured the potential difference between grounded ends of each wire. The natural potential difference that always occurs while a pair of grounded electrodes is connected was compensated at the inputs of the recorder by means of a potentiometer circuit. The bandwidth of sensors was in an interval from 0 to 220 Hz. Such a system allows us to control all three components of the low-frequency electromagnetic field.

The magnetic field perturbations were also recorded during a series of nuclear tests in 1961. The magnetic coils with vertically directed axis were used to perform the measurements of vertical component of the magnetic perturbation. Eight turns of wire were winded round the frame of coils, whose size was from 7.5 to 18.6 m. The eigenfrequency of electromagnetic vibrations of the coil was within 10–20 kHz, and these values significantly exceed the typical frequencies of the EMP.

Magnetic antennas with horizontal axis measured the horizontal component of magnetic field variations. The coils have an area of 2 m^2 area and 3.2×10^4 turns that correspond to the eigenfrequency about 60 Hz. The other kind of coils are 1 m^2 area, 7×10^3-turn loop of wire, so that the eigenfrequency is 200 Hz. A variety of amplifiers and filtering schemes were used to give the maximum of signal-to-noise ratio.

The EMP signal recorded at a proving ground in Nevada in 1958 during one of five underground explosions of the Hardtek series is depicted in Fig. 11.2. The depth of this explosion was 254 m, and trinitrotoluene/TNT equivalent was 19 kt (kiloton) (Zablocki 1966). What draws first attention is almost complete polarization of the electric field in the direction of azimuthal component, E_φ, and this feature was practically observed in all the tests.

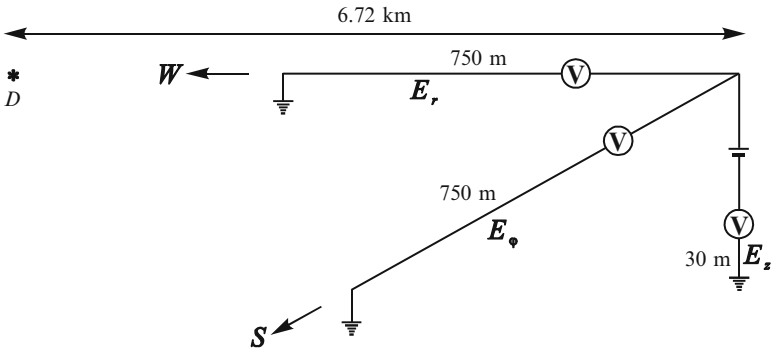

Fig. 11.1 A schematic plot of the equipment arrangement used during Hardtack II series of nuclear testing. The detonation hypocenter is marked by D. Adapted from Zablocki (1966)

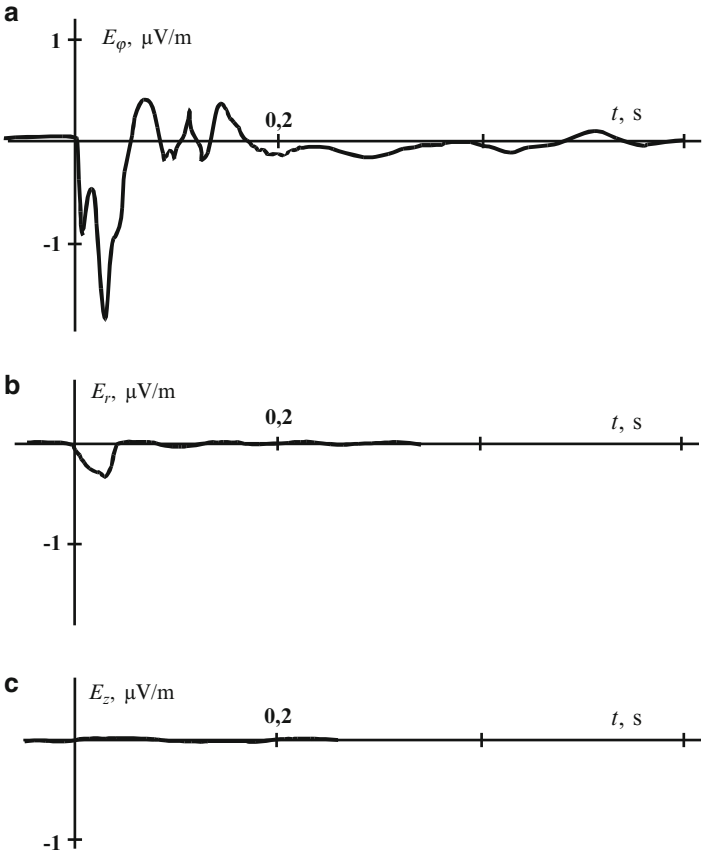

Fig. 11.2 A schematic plot of (**a**) tangential, (**b**) radial, and (**c**) vertical components of electric field variations measured at the proving ground in Nevada in 1958 during one of five underground explosions of the Hardtek series. The measurements were performed at 6.72 km distance east of explosion point and magnetic meridian. Adapted from Zablocki (1966)

The summary of the characteristics of majority of the signals could be made in the following way. The rise time of the initial spike is about 8–15 ms, and the polarization of perturbations is so that the vector of electric field is predominantly directed from South to North (Fig. 11.1). Within the time interval of 30–70 ms the field decreases approximately exponentially. Powerful detonations, as a rule, are accompanied by the shock excitation of the irregular vibrations lasted nearly 0.4 s. These vibrations reach 20 % of the signal magnitude (for example, see Fig. 11.2a). On numerous occasions the initial positive spike was followed by the negative half-wave with duration from 0.5 to 1 s as shown in Fig. 11.3 a, b with lines 1. The power spectrum of the EMP has spikes in the frequency ranges of 2–8 and 20–30 Hz. Besides the power spectrum tends to increase with decrease in frequency, which are lower than 2 Hz.

One more example is the nuclear test referred as "Bilbi," which was detonated at the depth of 714.5 m on September 1963. This contained underground explosion had a TNT equivalent $Y = 235$ kt, i.e. more than that considered above by one order of magnitude (Zablocki 1966). In this case the amplitude of electric field component, E_φ, was 3.6 μV/m at the distance 7.62 km to the South (along the magnetic meridian) of the detonation epicenter point. The rise time of the initial spike of the EMP did not exceed 15 ms and the time of the decrease down to zero level was approximately 150 ms. Notice that the rise time of the initial spike varies within 8–15 ms for all the tests. This value is larger than that of atmospherics, whose typical build-up time does not exceed 5 ms.

The relaxation time, τ_r, of the electric component of EMP as observed in the series of experiments is shown in Fig. 11.4 as a function of TNT equivalent, Y, of the detonation. This empirical dependence can be approximated by the following:

$$\tau_r = 30Y^{1/3} \text{ ms}, \tag{11.1}$$

where Y is measured in kt (1 kt is approximately equal to 4×10^{12} J).

The magnitude of electric field variations decreases approximately inversely proportional to the cubed distance, at least as the distance is smaller than 10 km. The empirical dependence of the horizontal component of electric field on the epicentral distance and TNT equivalent is given by (Zablocki 1966):

$$E = 2.2 \cdot 10^2 Y^{0.44}/R^3, \quad \mu\text{V/m}. \tag{11.2}$$

where the distance R is measured in kilometers. The typical magnitude of electric field can reach several tens mV/m under the detonation with TNT equivalent smaller than 150 kt (Malik et al. 1985; Sweeney 1989).

It is usually the case that the magnetic component of the EMP by nuclear underground explosions varies from several pT to several nT at the epicentral distances which are no more than 10 km. For example, the magnetic measurements during the detonation "Hardin" at the testing area in Nevada in 1987 have shown that

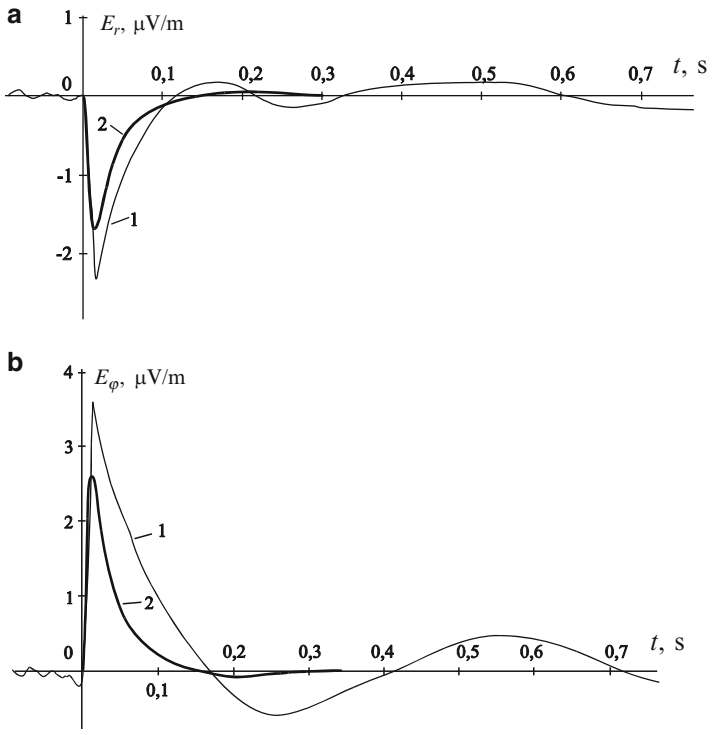

Fig. 11.3 Radial E_r (**a**) and azimuthal E_φ (**b**) components of electric field at the epicentral distance of 7.62 km from the explosion. (*1*) Experimental observations during the underground explosion "Bilbi" performed at the depth 714.5 m (Zablocki 1966); (*2*) Numerical calculations based on the model of expanding plasma ball (Ablyazov et al. 1988)

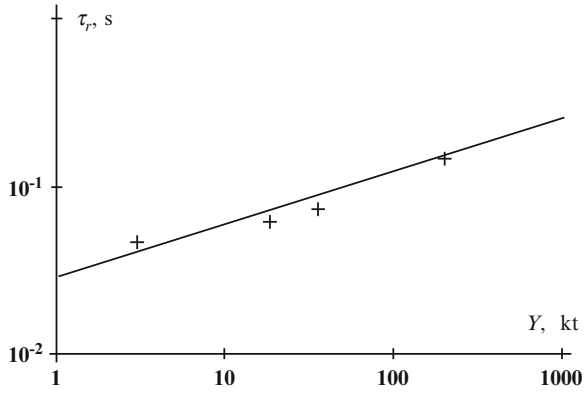

Fig. 11.4 Relaxation time of the electric component of EMP observed in a series of the experiments versus TNT equivalent of the detonation. Adapted from Zablocki (1966)

the magnitude of horizontal component of magnetic perturbations decreased from 40 pT at the distance of 5 km to 10 pT at the distance of 11 km from the detonation point (Sweeney 1989). At the same time the vertical component of the magnetic perturbations exceeded several hundreds pT.

The natural ULF electromagnetic background due to the atmospherics, the ionospheric and magnetospheric micropulsations and others restricts the possibility for detection of the EMP. As the distance is of the order of or much greater than 10 km, it appears that the EMP becomes undetectable because of small value of the signal-to-noise ratio. Moreover, the instability of the signal polarization produces the additional difficulty in the utilization of the cross-correlation technique to separate the signals from the background noise (Sweeney 1989, 1995, 1996). However the duration of initial part of the EMP can be utilized in order to estimate the energy of nuclear underground explosions (Gorbachev et al. 1999a,b).

11.1.2 Physical Mechanisms of EMP Caused by Atmospheric and Space Nuclear Explosions

At first let us consider possible physical mechanisms of the EMP under the atmospheric explosion. This effect can be due to the generation of radial currents of Compton recoil electrons originated from the short-term interaction ($\sim 0.25\,\mu s$) between the gamma-quantums of nuclear detonation and environment (Kompaneets 1958). It is known that approximately 0.03 % of the whole energy of the explosion is transformed into gamma-quantum radiation (Karzas and Latter 1962a,b). The average gamma-quantum energy is 1 MeV, and about 7.5×10^{21} gamma-quantums are generated per 1 kt of the TNT equivalent of the explosion. The gamma-quantums interact with the matter of nuclear device and with the molecules of air that causes the electron fluxes due to the Compton effect. On average the vectors of the electron velocities coincide with the directions of gamma-quantums motion. The radial electric current is also attributed to the photoelectrons resulted from X-rays emitted by the heated matter of the nuclear device.

Every Compton's electron ionizes the medium that leads to the generation of a great number of ion pairs. For example, the electron with kinetic energy of 2 MeV gives rise to approximately 3×10^4 pairs of ions in the air. In the air the free electrons are captured by molecules of O_2 having great chemical affinity with electrons. Under normal conditions the characteristic time of the electron attachment to molecules O_2 is about $0.01\,\mu s$. As a result, the reverse ionic current is developed thereby producing the relaxation of the dipole moment and radiation of electromagnetic waves in the frequency range around 10 kHz (Troitskaya 1960; Latter et al. 1961b; Gilinsky 1965; Gilinsky and Peebls 1968; Medvedev et al. 1980).

If the explosion gives rise to the spherically symmetrical system of currents and electric charges like the spherical condenser, then the electromagnetic field is strongly equal to zero outside this system. Actually always there are some causes for the non-symmetrical gamma-quantum spatial distribution. The irregularities of the gamma-quantum flux can be due to the construction features of the nuclear device or they could be excited by nonuniformity and anisotropy of the medium in which the gamma-quantums move. The asymmetry of gamma-quantum fluxes results in the asymmetrical distribution of the currents caused by Compton's electrons which in turn give rise to the generation of the dipole moment of the current system. The evolution of the dipole moment defines the temporal dependence of the EMP at far distance from the explosion site. However Latter et al. (1961) have noted that at the distances about several thousands kilometers from the detonation point the spectrum of the signals radiated by the atmospheric nuclear detonation is practically the same as that of typical atmospherics.

Leypunskiy (1960) has assumed that the EMP of the atmospheric nuclear detonation could be radiated because of the GMP caused by the fast extension of strongly heated plasma generated by the detonation. Since the plasma conductivity is so high as 10^3 S/m, the plasma motion in the geomagnetic field gives rise to the generation of electric currents, which screen the geomagnetic field. This results in the displacement of the geomagnetic field lines by the expanding plasma from the ionized area into the surrounding space. Such an effect which is often referred to as the "magnetic bubble effect," is followed by a subsequent current relaxation after the arrest and cooling of the plasma. These processes are accompanied by the radio-emission of the magneto-dipole type (Karzas and Latter 1962a; Kompaneets 1977). Additional effects can be due to the secondary gamma-quantums resulted from inelastic scattering and capture of the thermal neutrons by nuclei of atoms in the molecules of air and explosion products. A lot of aspects of the excitation of electromagnetic fields due to gamma and neutron radiation have been studied (e.g., see Sandmeier et al. 1972; Medvedev and Fedorovich 1975). The EMP of nuclear explosions in the outer space is different from that in the atmosphere in respect to the great value of mean free path of gamma-quantums and electrons. Johnson and Lippman (1960) and Karzas and Latter (1962b, 1965) have pointed out that the electrons in a so high-rarefied medium can produce cyclotron radiation in the Earth's magnetic field.

11.1.3 GMP Due to a Strongly Heated Plasma Ball Produced by Underground Explosions

The gamma radiation of the underground nuclear explosion is resulted from the fission of atomic nuclei, directly, as well as from the inelastic scattering of neutrons in the material of nuclear device and in the rock surrounding the underground chamber. Considering the Compton electrons mechanism of the EMP, we note

that in the ground the free path lengths of the gamma-quantums and electrons are significantly shorter than those in the air. In the case of Compton interaction the mean free path of quantum with energy on the order of 1 MeV is $\lambda_\gamma = b_\gamma/\rho$ where $b_\gamma \approx 1.5 \times 10^2\,\mathrm{kg/m^2}$ and ρ is the medium density. For example, one can find that $\lambda_\gamma \approx 100\,\mathrm{m}$ at the sea level in the atmosphere and $\lambda_\gamma \approx 0.1\,\mathrm{m}$ in the ground with the density $\rho = 1.7 \times 10^3\,\mathrm{kg/m^3}$. The free path length of the Compton electrons in the ground is $\lambda_e = b_e/\rho \approx 1\,\mathrm{mm}$ ($b_e \approx 2\,\mathrm{kg/m^2}$), i.e. this value is small too. Based on these simple estimates one may expect that the ratio of linear sizes of the electric dipoles caused by underground and atmospheric explosions with the same energy is inversely proportional to the ratio of densities of the corresponding media, i.e. 1–10^3. For the more accurate estimate we should take into account radiation-induced conductivity of the rock around the underground chamber.

One more significant factor which may greatly decrease the EMP of an underground explosion is the natural conductivity of the rock. The gamma-quantum pulse originated from the nuclear fission has a duration about 0.1 μs, which corresponds to the characteristic frequency $\omega \approx 10^7\,\mathrm{Hz}$. Taking a typical value of the rock conductivity $\sigma = 10^{-2}$–$10^{-3}\,\mathrm{S/m}$, we obtain the estimate of the corresponding skin-depth in the ground $r_s \sim (\mu_0\sigma_e\omega)^{-1/2} \approx 3$–$9\,\mathrm{m}$. To illustrate this strong attenuation, we note that if the explosion point is situated at the depth of 500 m, then this short signal can attenuate 10^{24} times or larger.

One more effect can be associated with the neutrons produced by explosions and by secondary gamma-radiation. The deceleration of these neutrons down to thermal energy is basically due to the interaction of the neutrons with nuclei of the light elements such as hydrogen. This seemed entirely possible since the ground usually contains about 16 % of hydrogen, 57 % of oxygen, 19 % of silicon, and 8 % of aluminum (Straker 1971). The duration of the deceleration process is on the order of 10 ns, whereas the life time of the thermal neutrons in the ground is about 0.1–1 ms that is significantly greater than the duration of primary gamma-quantum pulse. The inelastic scattering and capture of the thermal neutrons by the nuclei of aluminum and silicon causes the secondary gamma-radiation followed by the generation of electric current. The characteristic frequencies of this process are $\omega = 10^3$–$10^4\,\mathrm{Hz}$. This means that this effect could be observed in principle since the corresponding skin-depth is about 90–900 m, that is compared with the explosion depth.

The high-temperature plasma in the underground explosion cavity is believed to be one of the main sources for the EMP generation during a nuclear detonation. In the nuclear device the fission reaction is completed for the times about 10^{-8}–10^{-7} s. By this moment the matter still occupies the volume of about several cubic centimeters. Since the temperature of fissioned matter reaches 10^7 K, the atoms of light elements are completely ionized. This indicates that the electron-ion collisions prevail in the plasma. In such a case the conductivity σ_p of two-component plasma can be written in the form (e.g., Lifshitz and Pitaevskii 1981):

$$\sigma_p = \frac{4\sqrt{2}}{\pi^{3/2}} \frac{T^{3/2}}{Ze^2 m_e^{1/2} L}. \tag{11.3}$$

Here T is the plasma temperature measured in energy units, Ze is the charge of ions, m_e is the electron mass, and L is the Coulomb logarithm (Gaussian system of units)

$$L = \begin{cases} \ln \frac{r_D T}{Ze^2}, & \frac{Ze^2}{u\hbar} \gg 1; \\ \ln \frac{r_D (m_e T)^{1/2}}{\hbar}, & \frac{Ze^2}{u\hbar} \ll 1; \end{cases} \tag{11.4}$$

where $r_D = \left\{T/\left(4\pi n_e e^2\right)\right\}^{1/2}$ is the Debye shielding radius, n_e is the electron number density, u is the average relative velocity of electrons and ions, and $\hbar$ is the Plank constant. Substituting the average charge of ions $Z = 2$, the initial temperature $T = 1$–$10\,\mathrm{keV}$ and parameter $L = 4$ into Eqs. (11.3) and (11.4) we obtain the value $\sigma_p \approx 4 \times 10^7$–$1 \times 10^9\,\mathrm{S/m}$ which is close to the conductivity of metals under normal conditions.

The perturbations of the Earth magnetic field can diffuse in the conducting plasma according to Eq. (7.7). Let R be the radius of the underground chamber filled with the plasma. Then the characteristic time of the diffusion of GMPs inside the plasma ball can be estimated as follows:

$$\tau_d \approx \mu_0 \sigma_p R^2/4. \tag{11.5}$$

Taking the above value of σ_p and $R = 1\,\mathrm{m}$ one can find that $\tau_d \approx 10^8$–$10^9\,\mathrm{s}$, while the characteristic time of the plasma extension is about $t_p \approx 10$–$100\,\mathrm{ms}$ depending on the energy of explosion. Since $\tau_d \gg t_p$ the Earth magnetic field lines are completely frozen to the conducting plasma, so that the field lines move together with the plasma. Thus the plasma motion results in the local distortion of Earth's magnetic field. The equidistant lines of undisturbed magnetic field $\mathbf{B}_0$ are schematically shown in Fig. 11.5a while Fig. 11.5b displays a picture resulted from expansion of the conducting plasma ball.

Since the "frozen in" magnetic field is a uniform one in the plasma ball, the conservation of the magnetic field flux can be written as $B_0 \pi R_0^2 = B\pi R^2$ whence it follows that

$$B = B_0 R_0^2/R^2, \tag{11.6}$$

where B is the induction of uniform magnetic field into the ball with current radius R and R_0 is the initial radius of the ball. The perturbation, $\delta\mathbf{B}$, of the magnetic field in the ball is given by

$$\delta\mathbf{B} = \mathbf{B} - \mathbf{B}_0 = -\left(1 - R_0^2/R^2\right)\mathbf{B}_0. \tag{11.7}$$

If the ground conductivity around the plasma ball can be neglected, then the magnetic perturbations out of the plasma ball is described by the field of the effective magnetic dipole given by Eq. (7.5) where one should replace $\mathbf{B}$ by $\delta\mathbf{B}$. The magnetic dipole moment $\mathbf{M}$ is directed oppositely to the vector $\mathbf{B}_0$ and this absolute value

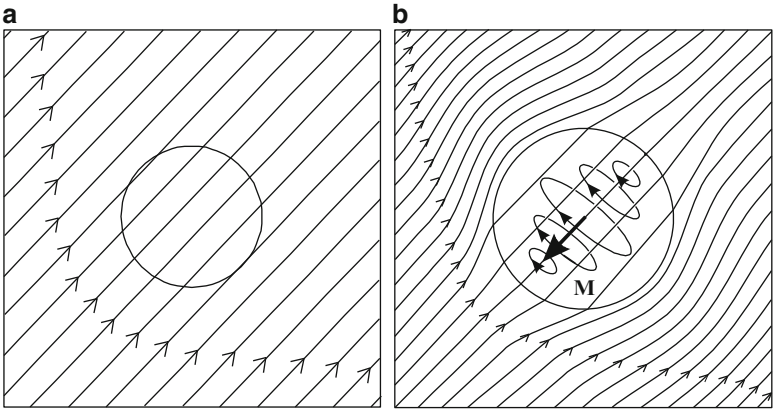

Fig. 11.5 Distortion of the geomagnetic field lines caused by the expansion of a highly heated plasma ball. (**a**) Equidistant field lines of undisturbed magnetic field $\mathbf{B}_0$; (**b**) Field line pattern resulted from the conducting plasma motion. The *closed "circular" lines* indicate the currents induced in the plasma ball. The effective magnetic moment is shown with vector **M**

depends on the current system in the plasma. In order to find the value of this moment we use the boundary condition which requires the continuity of the normal component of $\delta\mathbf{B}$ at the plasma ball surface. Equating the normal component of magnetic perturbations in Eq. (11.7) with that given by Eq. (7.5) at $r = R$, we obtain

$$\mu_0 M/\left(2\pi R^3\right) = \left(1 - R_0^2/R^2\right) B, \tag{11.8}$$

hence it follows that the effective magnetic moment of the plasma ball is

$$\mathbf{M} = -\frac{2\pi \mathbf{B}_0 R^3}{\mu_0}\left(1 - \frac{R_0^2}{R^2}\right). \tag{11.9}$$

Substituting Eq. (11.9) for **M** into Eq. (7.7) one can find the radial δB_r and tangential δB_θ components of the GMPs

$$\delta B_r = -B_0 \frac{R^3}{r^3}\left(1 - \frac{R_0^2}{R^2}\right)\cos\theta, \tag{11.10}$$

$$\delta B_\theta = -B_0 \frac{R^3}{2r^3}\left(1 - \frac{R_0^2}{R^2}\right)\sin\theta. \tag{11.11}$$

Here θ is the polar angle measured from the direction of $\mathbf{B}_0$.

As is seen from Eqs. (11.10) and (11.11) the magnitude of EMP decreases with distance inversely proportional to the distance cubed. Substituting the following numerical parameters $B_0 = 5 \times 10^{-5}\,\mathrm{T}$, $R = 30\,\mathrm{m}$, $R_0 = 1\,\mathrm{m}$, and $r = 7\,\mathrm{km}$

into Eqs. (11.10) and (11.11) we get the estimate $\delta B \approx 4\,\mathrm{pT}$ which is consistent in magnitude with the signals observed during underground detonations. At the distance exceeding approximately 10 km, the amplitude of the signals falls off below the level of background noise.

The maximal radius R of the explosion cavity is proportional to $Y^{1/3}$ where Y is the TNT equivalent of the explosion (e.g., see Chadwick et al. 1964; Rodionov et al. 1971). This implies that the magnitude of the GMPs in Eqs. (11.10) and (11.11) is proportional to Y. The similar relationship holds true for the electric field variations that contradicts the empirical dependence given by Eq. (11.2). This means that the simplified model considered above does not describe the EMP effect quite adequately.

To estimate the EMP relaxation time due to return diffusion of the magnetic field into the plasma, we now suppose that the cooling of the uniformly expanding plasma follows the adiabatic law. The adiabatic equation of a perfect gas reads

$$TR^{3(\gamma-1)} = T_0 R_0^{3(\gamma-1)}, \tag{11.12}$$

where γ stands for the adiabatic exponent and the subscript zero is related to the initial values of the plasma temperature and the radius of underground cavity. Considering the moment of the cavity stoppage and substituting the numerical values $R/R_0 = 30$ and $\gamma = 5/3$ into Eqs. (11.3), (11.4), and (11.12), we find that at this moment the plasma temperature and conductivity are $T \approx 1$–$10\,\mathrm{eV}$ and $\sigma_p \approx 1.5 \times 10^3$–$4 \times 10^4\,\mathrm{S/m}$. Substituting these values into Eq. (11.5) gives the rough estimate $\tau_d \approx 0.4$–$10\,\mathrm{s}$ which is compatible with the duration of the EMP signals shown in Figs. 11.2 and 11.3.

In the strict sense, the amplitude estimates given by Eqs. (11.10) and (11.11) are valid in the extreme case of a perfectly conducting plasma ball. To study the effect of finite plasma conductivity we consider the expanding uniform plasma ball situated in the rock at higher depth. The conductivity and radius of the plasma ball are assumed to be given functions of time; that is $\sigma_p = \sigma_p(t)$ and $R(t) = R_0\beta(t)$, where R_0 is the initial ball radius (Ablyazov et al. 1988). In this model the rock conductivity is much smaller than the plasma one. A detailed analysis of this problem presented in Appendix I has shown that the ULF GMPs outside the ball can be qualified as magnetic dipole field. The solution of the problem is represented as a series with respect of eigenfunctions of the problem. The effective magnetic moment of the plasma ball can be found from Eq. (11.80)

$$\mathbf{M}(t) = -\frac{12R_0^3\mathbf{B}_0\beta(t)}{\pi\mu_0}\sum_{n=1}^{\infty}\frac{1}{n^2}\int_0^t\frac{d\beta^2}{dt'}\exp\left(-\int_{t'}^t\frac{\pi^2n^2}{\mu_0\sigma_p R_0^2\beta^2}dt''\right)dt'. \tag{11.13}$$

In the limit $\sigma_p \to \infty$ we get

$$\mathbf{M}(t) = -\frac{12\zeta(2)R_0^2R(t)\mathbf{B}_0}{\pi\mu_0}\left(\frac{R^2(t)}{R_0^2}-1\right), \tag{11.14}$$

where $\zeta(x)$ denotes the ζ-function of Riemann. Taking into account that $\zeta(2) = \pi^2/6$ we obtain that Eq. (11.14) for $\mathbf{M}$ coincides with Eq. (11.9) which was derived in the same extreme case. In the opposite case $\sigma_p \to 0$ we have a so apparent result $\mathbf{M} = 0$.

The low-frequency conductivity of the heated plasma is defined by Eqs. (11.3) and (11.4) because the electron-ion collisions prevail over other ones at high temperature. Suppose that the plasma is the perfect gas that expands according to the adiabatic law (11.12). Then the plasma temperature varies as $T = T_0/\beta^{3(\gamma-1)}$ where T_0 is the initial plasma temperature. Now we first examine the exponent function under the integral sign in Eq. (11.13). The expression standing in the index of the exponent function can be written in the form (Gaussian system of units)

$$\frac{\pi c^2 n^2}{4\sigma_p R_0^2 \beta^2} = \frac{n^2}{\tau_d}\left(\frac{\beta}{\beta_m}\right)^{\mu}, \tag{11.15}$$

where

$$\tau_d = \frac{16\sqrt{2}}{\pi^{5/2}} \frac{R_0^2 T_0^{3/2}}{Ze^2 L c^2 m_e^{1/2} \beta_m^{\mu}}, \qquad \mu = \frac{9\gamma - 13}{2}. \tag{11.16}$$

Here c is the light speed in the free space and β_m denotes maximum of the function $\beta(t)$; that is $\beta_m = R_m/R_0$, where R_m is the final radius of the plasma. The parameter τ_d determines the back diffusion time of the perturbed magnetic field into the plasma ball. This parameter has the same sense as the relaxation time given by Eq. (11.5). It can be shown that Eq. (11.16) coincides with Eq. (11.5) within a constant factor. Substituting the numerical parameters $R_0 = 1\,\text{m}$, $T_0 = 1\,\text{keV}$, $Z = 2$, $L = 4$, $\gamma = 5/3$ and $\beta_m = 30$ into Eq. (11.16) we obtain $\tau_d = 0.55\,\text{s}$. This value is compatible with the relaxation time of EMP observed during underground explosions. However the dependence $\tau_d \propto Y^{2/3}$ which follows from Eq. (11.16) contradicts with the empirical dependence $\tau_d \propto Y^{1/3}$ displayed in Fig. 11.4.

There are a lot of factors which may affect the electromagnetic signals under the explosions and thus may concern this discrepancy. For example, the melting and evaporation of the surface of an underground chamber subjected to the radiation of nuclear explosion results in changing the plasma constituents due to the injection of evaporated particles. A fall in plasma temperature brings the decrease in the plasma ionization degree due to recombination process. These effects lead to the changes in the plasma conductivity, adiabatic exponent, and other plasma parameters that leave out of account in the above models.

The changes in the underground chamber size can be approximated by a smooth function, for example,

$$\beta(t) = 1 + (\beta_m - 1)\left[1 - \exp\left(-t/\tau_b\right)\right], \tag{11.17}$$

where τ_b is the characteristic time of chamber expansion. In Fig. 11.3 the data recorded during the containing underground explosion "Bilbi" (Zablocki 1966) are compared with the numerical calculations which are based on the above model and Eq. (11.17) (Ablyazov et al. 1988). As is seen from this figure, the theoretical dependencies shown with lines 2 are in qualitative agreement with the observations shown with lines 1. The vibrations followed by the initial spike can be explained by the hydrodynamical instability of the expanding plasma. Hydrodynamic waves excited in the plasma and products of detonation can be reflected from the walls and center of the chamber thereby producing the modulation of the EMP signals in amplitude and frequency (Gorbachev et al. 1999). It should be noted that in specific events the EMP exhibits the polarization corresponding to the field of a magnetic dipole whereas the polarization in other cases is rather close to the electric dipole one.

11.2 Electromagnetic Effects Due to Shock Wave (SW) and Rock Fracture

11.2.1 Electric Dipole Moment Due to Shock Polarization of Rocks

A SW generated by the contained underground explosion gives rise to rock polarization which in turn can serve as a possible source for the electric dipole (Surkov 1986). The shock polarization effect in laboratory conditions have been studied in any detail in Sect. 9.1. Here we deal with large-scale polarization phenomena under the natural situation. There are a few stages of the deformation and rock fracture caused by an underground explosion. At first the fast expansion of the underground chamber due to plasma impact and vaporation of the chamber walls results in the generation of the strong SW with pressure amplitude $\sim 10^{11}$–10^{12} Pa (e.g., Zeldovich and Raizer 1963; Chadwick et al. 1964; Rodionov et al. 1971; Baum et al. 1975). At this stage called as hydrodynamical one the rock strength can be neglected, and the pressure amplitude decreases with distance as r^{-3} over a length of several meters or tens meters. During this stage the pressure falls off by 3–4 order of magnitude, and then the amplitude attenuation obeys the law r^{-n}, where $1 < n < 2$. As before the shear stress will exceed the crushing strength of the rock so that the fracturing of rocks occurs behind the SW front. Then the crushing wave begins to decelerate and thus fails to keep up with the main shock so that the primary wave is split into two waves. At the moment of the crushing wave stop the radius of zone of complete fracturing reaches tens or hundreds meters depending on the energy of explosion. The tension stresses take place in the region between the fracturing zone and the SW front. Since these stresses exceed the ultimate tensile strength, there develop the radial cracks in this region. Typically the

zone of intensive radial fracturing is as much as several hundreds meters in length. When the wave amplitude falls off below the rock strength, the medium behaves like elastic one. At this stage which is referred as the seismic one, the SW transforms into the elastic/seismic wave. If the dispersion-dissipative properties of the rock are not important, then the amplitude of the longitudinal seismic wave decreases with distance as r^{-1}. When this wave reflects from the day surface, it is split into the primary/longitudinal (P-wave), secondary/transverse (S-wave) and surface Rayleigh and Love waves.

In this brief overview we have omitted a few details of camouflet underground explosions such as the generation of the unloading wave, dilatancy of the fractured rock, dynamics of the camouflet chamber and etc.

The stress wave propagating in the ground and rocks is known to generate a variety of low-frequency electromagnetic phenomena so that the interpretation of the observation is often troublesome. One source of this variety is that the natural materials and rocks are very inhomogeneous as for their rheological structure and electrical parameters. For example, the ground conductivity strongly depends on the humidity and porosity which vary with depth. The rock fracturing and pore collapse caused by the SWs gives rise to the generation of the local electric fields and great charges near the cracks and pores that can be accompanied by the local electric breakdowns of the medium.

Now we discuss the existence of the shock polarization effect in nonuniform media at different structural levels (Surkov 2000). Firstly, the microscopic movements of the charged dislocations and point defects can result in the polarization of individual monocrystals and grains. This effect is enhanced essentially in the vicinity of the grain boundaries, microcracks, small inclusions, and pores. Secondly, considering the macroscopic scale we note that the polarization processes are localized in the regions of enhanced stresses; that is, near tips of large cracks and individual blocks of fractured rock. So one may expect that there exists certain hierarchy of relaxation times of the shock polarization. The largest values of the rise and decay times of the shock polarization can exceed by several orders of magnitude the same parameters observed under laboratory tests. Thus, we come to the conclusion that the SW generates its own, as a rule, low-frequency electromagnetic field due to the polarization of different structural units of nonuniform matter.

In what follows we assume the linear dependence between the rock polarization Π and the amplitude of pressure P_m (Allison 1965)

$$\Pi = \alpha P_m \left[1 - \exp\left(-\frac{t}{\tau_f}\right)\right] \exp\left(-\frac{t}{\tau_r}\right) \eta(t), \tag{11.18}$$

where α is empirical coefficient of proportionality, τ_f is the rise time, τ_r is the decay time of the polarization, and $\eta(t)$ denotes the step function.

The shape of the SW resulted from an explosion is very similar to a spherical one. Suppose that behind of the wavefront the matter is polarized in the radial direction. Besides the medium polarization has a weak asymmetry that can be due to an irregular distribution of fracturing, asymmetry of the shock wavefront,

influence of the gravity, presence of large-scale inhomogeneity of the medium and other causes. So, the actual distribution of the shock polarization is not entirely spherically symmetrical. For instance, we assume the cylindrical symmetry of such a distribution (Surkov 1986). The origin of coordinate system is placed in the center of symmetry of the spherical SW. The radial polarization of the medium is described by the following equation:

$$\mathbf{\Pi}_1 (r, \theta, t - t_a) = (1 + \beta \cos\theta)\, \Pi (r, t - t_a)\, \hat{\mathbf{r}}, \tag{11.19}$$

where β is the small parameter of asymmetry, $\hat{\mathbf{r}}$ is the unit vector and the parameter t_a denotes the moment of the SW arrival at the point with spherical coordinates r and θ. Here the polar angle θ is measured from the axis of symmetry z.

As has already been stated in Sect. 9.1, the SW in a solid carries the electric charge. Let R_0 be the initial radius where the primary charge of the SW is formed. By assuming that the SW velocity, U, is constant, we obtain that $t_a = (r - R_0)/U$. The pressure magnitude in the spherical SW changes with distance by a power law, i.e. $P_m = P_* (R_0/r)^n$, where P_* denotes the pressure magnitude at the radius $r = R_0$. For the ground the value $n \approx 1.6$ is usually accepted though the exponent n can vary depending on distance (e.g., see Rodionov et al. 1971). The actual values of the characteristic times τ_f and τ_r can be of the order of the SW duration. Since the width of shock wavefront in the ground can reach several meters, these parameters can be as large as a few ms or even more. In the model by Grigor'iev et al. (1979) the SW rise time is inversely proportional to the pressure magnitude and hence it follows that $\tau_f = \tau_0 (r/R_0)^n$ where τ_0 is the constant.

The vector of the dipole electric moment $\mathbf{d}$ of the polarized matter is directed along the axis of symmetry z. In order to find the absolute value of $\mathbf{d}$, one should integrate the projection of $\mathbf{\Pi}_1$ on z-axis over the volume V occupied by the SW, i.e. over the volume restricted by the radius $R_f = R_0 + Ut$

$$d(t) = \int_V \Pi_1 (r, \theta, t - t_a) \cos\theta \, dV. \tag{11.20}$$

Here we consider the time interval when the SW has not yet reached the ground surface.

The space charges due to the shock polarization of the medium are mainly situated in the vicinity of the shock wavefront in the layer with depth on the order of $U(\tau_r + \tau_f)$. These charges have a certain sign depending on the properties of the rock. The opposite charges are situated behind the SW front at the distance which is equal to the charge relaxation length or they are concentrated around the underground cavity. Certainly, in all cases the total electric charge contained in the rock is equal to zero.

Below we assume an inequality $U(\tau_r + \tau_f) \ll R_f$. Since the integral sum in Eq. (11.20) is mainly accumulated within a short length $U(\tau_r + \tau_f)$, the functions

$r^2\Pi\left(r, t-t_a\right)$ and $\tau_f\left(r\right)$ under the integral sign can be considered as constant values. Taking these function at $r = R_f$ and performing integrations yields

$$d\left(t\right) = \frac{4\pi\alpha\beta P_* R_0^2 \tau_r}{3\left(1+t/\tau_s\right)^{n-2}}\left[1-\exp\left(-\frac{t}{\tau_r}\right)-\gamma\left\{1-\exp\left(-\frac{t}{\gamma\tau_r}\right)\right\}\right] \tag{11.21}$$

Here we have introduced the auxiliary function

$$\gamma\left(t\right) = \frac{\tau_f\left(R_f\right)}{\tau_r+\tau_f\left(R_f\right)} = \frac{\tau_0\left(1+t/\tau_s\right)^n}{\tau_r+\tau_0\left(1+t/\tau_s\right)^n}, \tag{11.22}$$

where $\tau_s = R_0/U$. We notice that the spherically symmetric portion of Eq. (11.19) which is independent of θ does not contribute to the dipole moment in Eq. (11.21) at all. This obvious result follows the fact that the spherically symmetric charge distribution confined by two concentric spheres does not create the electromagnetic field in the outer space.

The dipole moment given by Eq. (11.21) determines the electromagnetic field of SW far away from the explosion point. The analysis of the near field spectrum caused by the SW has shown that the spectral intensity is enhanced in the vicinity of typical frequencies $\omega \approx \tau_r^{-1}$, $\omega \approx \tau_s^{-1}$ and $\omega \approx \tau_*^{-1}$ where $\tau_* = \tau_0\tau_r/\left(\tau_0+\tau_r\right)$ (Surkov 1986). This frequency range lies within an interval from several Hz to one kHz that is in a reasonable agreement with typical spectra of the EMP observed during large-scale underground explosions.

In Sect. 3.1.4 we have noted that in the atmosphere the vertical dipole antenna is a more effective radiator of electromagnetic waves than the horizontal one (see Fig. 3.5). By contrast, it follows from the theory that the horizontal component of the underground dipole antenna plays more significant role than the vertical component (Wait 1961, 1970). To clarify this statement we note that the vertical dipole generates a symmetrical distribution of electric current in the surrounding conductive space as shown in Fig. 11.6a. On the ground surface these currents flow in the radial directions from the point O. The effective electric dipole **d** of such a system of surface radial currents is equal to zero, which means that the effective antenna produced by these surface currents does not radiate. On the other hand in the case of the horizontal dipole, shown in Fig. 11.6b, the surface electric currents flow approximately along the direction of dipole vector **d**. These current systems are equivalent to the nonzero electric dipole turned to the same direction.

Thus, as a first approximation, the electromagnetic field generated by the SW of underground explosion is equivalent to that of horizontal component of the effective current dipole, which is usually assumed to be located in a homogeneous conducting half-space. The shape of the signals detected on the ground surface depends on both the function $d(t)$ given by Eq. (11.21) and the conductivity of the half-space. A theoretical analysis of this problem has shown that the EMP has a bipolar shape similar to that shown with lines 2 in Fig. 11.3 (Surkov 1986). In this model the first narrow spike is due to the fast variation of the shock-induced dipole moment

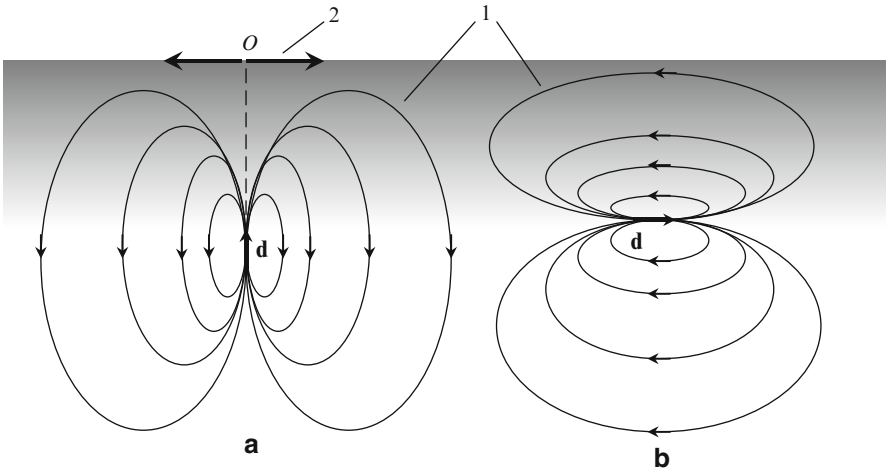

Fig. 11.6 Effective underground (**a**) vertical and (**b**) horizontal dipoles **d** produced by electric current systems in the homogeneous conducting ground. *1*—current field lines, *2*—radial currents on the ground surface

for the time of the order of $\tau_r + \tau_f$ while the negative half-wave is caused by the subsequent attenuation of the SW amplitude. The predicted amplitudes of the EMP at the distances 5–10 km are on the order of several μV/m and 1–10 pT, which is also compatible with observations though the duration of the observed signals is greater than calculated values.

It appears that the EMP is a combined effect resulted from different sources such as the high-temperature plasma ball, SW polarization, and perhaps gamma and neutron radiations. There are a few difficulties in distinguishing these sources because the direction of the shock-induced dipole is unknown prior to the test; that is, the dipole direction can be accidental in character.

11.2.2 Residual Electromagnetic Field on the Ground Surface

In what follows we examine the phenomena arising after the abatement of the EMP. The residual quasi-static magnetic perturbations at the epicenter of surface and buried detonations have been observed by Stacey (1964) and by Undzenkov and Shapiro (1967). One of the first measurements of residual magnetic field has been made in the region Medeo (USSR) at the distance of 700 m from the detonation point (Barsukov and Skovorodkin 1969). The detonation was made in granite, whose natural magnetization was $J = 5$–100 mA/m. The ground-based observation showed that 1 h 50 min after the moment of detonation the local geomagnetic field changes by 8 nT and this perturbation is halved 5 h after it. The field relaxation

back to the former level was lasted during 24 h. Hasbrouk and Allen (1972) have reported magnetic measurements during the underground nuclear explosion, which is referred to as CANNIKIN experiment. The explosion with TNT equivalent of 5 Mt was conducted on the Amchitka Island (Aleutian Islands) on January 6, 1971. The proton magnetometer, which was placed at the epicentral distance of 3 km, recorded the gradual increase of the magnetic field by 9 nT in 30 s after the detonation. The field variation about 2 nT was detected at the distance of 9 km. The magnetic survey around the epicenter of detonation revealed that the 10 nT changes of the geomagnetic field were kept approximately constant for 8 days.

Thus the magnetic perturbations due to the detonation in rock could be conventionally divided into three stages (Erzhanov et al. 1985): (1) the transient alternating-sign pulse (EMP) with duration smaller than 1 s and with magnitude 0.1–100 nT; (2) the 10–20 nT residual changes which can relax during several hours or days; (3) the long-term residual changes with magnitude of several nT that can last for several days or months.

It was hypothesized by Stacey (1964) and by Undzenkov and Shapiro (1967) that the residual magnetic perturbations near the detonation site are excited by means of changes in the natural rock magnetization which in turn are based on the occurrence of inelastic/plastic deformations in the rock. As noted in Sect. 9.1, the laboratory tests with magnetite-bearing rocks have shown that the sample magnetization can change by 1% under the stress of 10 MPa. Restoration of the local geomagnetic field back to the former level could be resulted from the relaxation of inelastic deformation in the rock. However this effect is likely if the rock contains sufficient amount of the ferromagnetic inclusions.

To estimate the above effect, we consider the model in which the SW and residual stresses around the detonation site are spherically symmetric (Surkov 1989). The SW magnitude exceeds the crushing strength of the rock in the vicinity of the powerful explosion. The crushed zone is assumed to have a spherical shape with radius of R_c. As a rule this radius is of the order of several tens meters. The residual magnetization in this zone is probably chaotic owing to the repacking of the broken rock. Therefore the contribution of this zone to magnetic perturbations is neglected as compared to the residual rock magnetization which occurs in the region $r > R_c$. In this region the SW magnitude is lower than the crushing strength but higher than the tensile strength of the rock. The medium is monolithic in character while there occur separate large cracks. The typical size of this region is of the order of several hundreds meters, and the rock deformation is elastic and reversible from outside of this zone.

The primary rock magnetization, $\mathbf{J}$, is assumed to be constant. In the region $r > R_c$ the magnetization increment, $\Delta\mathbf{J}$, due to the SW is described by Eq. (9.29), where $s_n = s_{rr}$ denotes the magnitude of radial component of the stress tensor. The stress magnitude depends only on the distance r from the explosion point. The effect of residual rock magnetization ceases at the certain radius $R_e > R_c$ when the stress magnitude falls short of certain threshold stress so that in the field $r > R_e$ the residual magnetization is absent. The magnetic permeability of the rock inside the zone $R_c < r < R_e$ can be slightly different from that of surrounding medium.

For simplicity we ignore this difference and set the magnetic permeability is equal to unity everywhere. The induction of remanent magnetic field, **B**, within the zone $R_c < r < R_e$ is described by the following Maxwell equation:

$$\nabla \times \mathbf{B} = \mu_0 \nabla \times \Delta \mathbf{J}. \tag{11.23}$$

The detonation point is chosen to be the origin of coordinate system with z-axis parallel to the vector **J**. Spherical coordinates, i.e. the radius r and the polar angle θ measured from z-axis are used. For the region $r > R_e$ the solution of Eq. (11.23) is given by Eq. (7.5) which describes the field of magnetic dipole. Taking Eq. (9.29) for $\Delta \mathbf{J}$ the effective magnetic moment of the magnetized rock can be written as follows:

$$\mathbf{M} = 4\pi C_m \mathbf{J} \int_{R_c}^{R_e} r'^2 s_{rr}\left(r'\right) dr', \tag{11.24}$$

where C_m denotes the piezomagnetic coefficient.

According to this model, far away from the detonation point the residual magnetic field decreases with distance as $B \sim r^{-3}$. However, this dependence contradicts the data obtained during the experiment referred to as MASSA (Erzhanov et al. 1985). The detonation of chemical high explosive (HE) with mass of 251 t was made on the sandstone surface. Survey of the changes of the geomagnetic field for this detonation was made at the different points in the distance range from 0.5 to 10 km. It was found that the decrease of the residual magnetic field is closer to the dependence $B \sim r^{-1}$ in character.

This discrepancy between the theory and experiment can be due to the fact that the observation point was located at the distances within $R_c < r < R_e$ where the remanent rock magnetization should occur (Surkov 1989). The solution of this problem is found in Appendix I. Since the elastic strain and stress are predominant in this region, the magnitude of the normal stress in the seismic wave satisfies the following law: $s_{rr}(r) = P_c R_c / r$, where the parameter P_c is of the order of the crushing strength or of tensile one. Substituting this expression into Eqs. (11.90) and (11.91) and performing integration, we obtain the solution of the problem $(R_c < r < R_e)$

$$B_r = \frac{\mu_0 C_m J P_c R_c \cos\theta}{r}\left(1 - \frac{R_c^2}{r^2}\right), \tag{11.25}$$

$$B_\theta = -\frac{\mu_0 C_m J P_c R_c \sin\theta}{2r}\left(1 + \frac{R_c^2}{r^2}\right). \tag{11.26}$$

As is seen from Eqs. (11.25) and (11.26), the magnetic field components decrease with distance slower than the rate expected from the dipole law. When $r^2 \gg R_c^2$, they decrease with distance approximately as r^{-1}. However, this solution provides

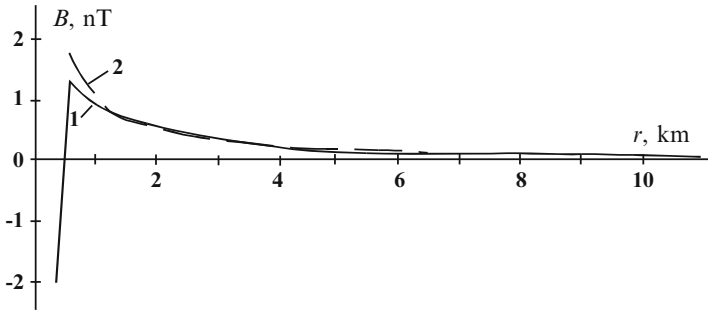

Fig. 11.7 Remanent changes in the Earth magnetic field resulted from the surface detonation of HE with mass 251 t as a function of distance from the detonation point. *1*—Experimental data (adapted from Erzhanov et al. 1985); *2*—model calculations (Surkov 1989)

only a rough estimate of the phenomenon because we do not take into account the effect of medium unloading near the free surface.

The remanent changes of the Earth magnetic field measured in the case of MASSA experiment are shown in Fig. 11.7 with line 1 (Erzhanov et al. 1985). The numerical calculation shown with the dotted line 2 was made under the following parameters: $P_c = 0.1\,\text{GPa}$, $C_m = 1\,\text{GPa}^{-1}$, $R_c = 100\,\text{m}$, and $J = 0.12\,\text{A/m}$. It is obvious from this figure that the theoretical and experimental dependencies are close except for the region of $r < 0.5\,\text{km}$. Actually the surface detonation generates the non-spherically symmetric SW. The study of such a problem has shown that the asymmetry of the rock magnetization can lead to an increase of the above estimate (Surkov 1989).

The additional effect can be due to the impact action on technical constructions and installations which are magnetized under the shock and vibrations in the Earth magnetic field. The mechanism of this effect has been discussed more fully in Sect. 9.1. One of such construction is the steel casing/encasement pipe which is used in order to protect utility lines from getting damaged and for lowering the explosive device in the rockhole. Vibrations of the casing pipe due to SW propagation can result in the pipe magnetization thereby producing local changes of the geomagnetic field.

One more effect can be due to the redistribution of natural and man-made telluric currents flowing in the rock around the place of underground detonation. The major origin for the man-made current is believed to be the electrochemical processes at the interface between the casing pipe and surroundings. The occurrence of the contact potential difference at the surface of the metallic pipes can be associated with the difference between mechanisms of conductivity, namely electronic conductivity in the metal and ionic one in the rock surrounding the pipe. It should be noted that the similar effect is usually observed in the vicinity of ore deposit (e.g., see Semenov 1974). The contact electromotive force at the casing pipe surface depends on the depth because the mineral content of underground water varies with depth. As a result the currents develop in both the casing pipe and the rock around the pipe.

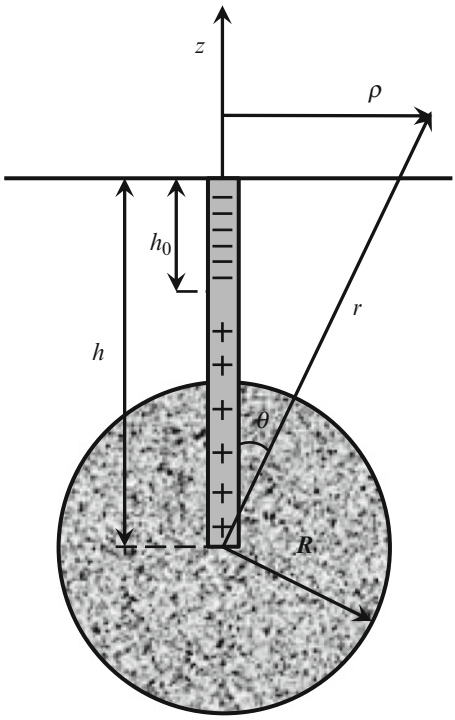

Fig. 11.8 Model distribution of contact EMF along the casing pipe. A *circle* indicates the boundary of fractured zone resulted from the explosion

The quasi-static electromagnetic perturbations originated from these currents could be detected just after the casing pipe installation and even before the underground detonation itself.

Considering the electrochemical processes around the metallic ore body, it is usually the case that the top of ore body plays a role of a negative electrode (Semenov 1974). In this notation, we suppose that the upper part of the casing pipe operates as a negative electrode while the lower part serves as a positive electrode. Let h be the length of casing pipe while h_0 be the length of the effective negative electrode as schematically shown in Fig. 11.8. The detonation at the depth h results in the formation of spherical region of the fractured rock with radius R, whose conductivity, σ_p, is different from the conductivity, σ_g, of the surrounding rock. Suppose that the current distribution is stationary and the total current, I, generated by the electrodes is a given value. The currents per unit length of negative electrode, I/h_0, and positive electrode, $I/(h-h_0)$, are constant values. Then the potential, φ, of the electric field is determined by Poisson equation which should be supplemented by the proper boundary conditions; that is, the potential and its derivative with respect to radius is continuous at the ball surface and the vertical component of the current density has to be zero at the free surface.

The solution of this problem for the potential φ can be represented in the form $\varphi = \varphi_0 + \varphi_p$, where φ_0 denotes the potential generated by the casing pipe in the

uniform conducting half-space with constant conductivity σ_g while φ_p stands for the perturbations caused by the appearance of the fractured region with conductivity σ_p. In the atmosphere ($z \geq 0$) the potential φ_0 reads

$$\varphi_0 = \frac{I}{2\pi\sigma_g (h - h_0)} \left\{ \ln \frac{\sqrt{(z + h_0)^2 + \rho^2} - z - h_0}{\sqrt{(z + h)^2 + \rho^2} - z - h} + \left(1 - \frac{h}{h_0}\right) \ln \frac{\sqrt{(z + h_0)^2 + \rho^2} + z + h_0}{\sqrt{z^2 + \rho^2} + z} \right\}, \tag{11.27}$$

where ρ denotes the polar radius shown in Fig. 11.8. The approximate relationship for the perturbations caused the rock fracture is given by (Surkov 1989)

$$\varphi_p = \frac{I\left(\sigma_g - \sigma_p\right)}{2\pi\sigma_g (h - h_0)} \sum_{k=1}^{\infty} \frac{\Lambda_k P_k (\cos\theta)}{k\sigma_p + (k + 1)\sigma_g} \left(\frac{R}{r}\right)^{k+1}, \tag{11.28}$$

where

$$\Lambda_k = \frac{2k + 1}{k + 1} - \frac{hR^k}{h_0 (h - h_0)^k} - \left(1 - \frac{h}{h_0}\right) \left(\frac{R}{h}\right)^k. \tag{11.29}$$

Here $P_k(\cos\theta)$ are Legendre's polynomials, $r = \left\{(z + h)^2 + \rho^2\right\}^{1/2}$, and the angle θ is shown in Fig. 11.8.

If $R \ll h$ and $R \ll h - h_0$, then Eq. (11.28) is simplified because only first term of the series can be taken into account. If, in addition, $\rho \gg h$,s then Eq. (11.27) is also simplified. For example, on the plane $z = 0$ the solution of the problem is reduced to

$$\varphi_0 = -\frac{I h (h + h_0)}{4\pi\sigma_g \rho^3}, \qquad \varphi_p = \frac{3I\left(\sigma_g - \sigma_p\right) hR^2}{4\pi (h - h_0)\sigma_g \left(\sigma_p + 2\sigma_g\right)\rho^3}. \tag{11.30}$$

It follows from Eq. (11.30) that both the casing pipe and fractured zone produce only a local effect since the electric field $\mathbf{E} = -\nabla\varphi$ falls off faster with distance, that is, as ρ^{-4}. The numerical estimates of this effect seem to be accident-sensitive because of the lack of information about actual values of the parameters I and h_0.

The magnetic perturbation in the ground has only the azimuthal component B_ϕ, owing to the symmetry of the given problem, though $B_\phi = 0$ in the atmosphere. Actually the magnetic perturbation is equal to a finite value near the ground surface because the symmetry of the problem gets broken due to asperity of the ground surface. Notice that the magnetic field associated with this effect and the field due to

shock magnetization are different in symmetry that enables us to distinguish these phenomena.

The irreversible deformation and fracture of rocks may greatly affect natural terrestrial currents which in turn result in the similar effects. There are a few causes for the terrestrial current generation such as variations of magnetospheric and ionospheric fields, electrochemical processes in the ground, groundwater flow, local hydrological factors, precipitations and etc. The shock impact on the rock leads to the changes in permeability of capillaries, channels, and fluid-filled cracks followed by the changes in rock conductivity.

The heated gaseous products of detonation contained in the underground cavity can produce thermoelectric and thermo-galvanomagnetic phenomena in the surrounding space. The heating of the medium and temperature gradient can save for the long times if the decay of radioactive elements contained in the detonation products goes on. These processes could also provide for stable changes of the local electromagnetic Earth's field in the vicinity of the detonation point.

11.2.3 Electric Field of Gas-Dust Clouds

Surface and shallow buried detonations are accompanied by dustfall and the ejection of broken ground. The explosion products and air heated by an explosion are mixed with fragments of the broken ground, thereby producing the gas-dust cloud which can emerge in the atmosphere by the action of buoyancy force. There are a few stages of the cratering explosion. At first the ground dome is developed under the influence of the explosion for subseconds to be followed by the gas break through the dome and by the gas output in the atmosphere. Then the air-SW is created in the atmosphere. The coarse fragments of the flying rocks follow ballistic trajectories, while fine particles are pulled into the gas motion behind the shock front. The gas-dust cloud rises upward during several seconds or minutes depending on the scale of explosion. The conventional time scale is several minutes or hours for the dust deposition and for the dispersal of gas-dust clouds.

The generation of the gas-dust cloud caused by an explosion is accompanied by the appearance of low-frequency (up to 100 Hz) electromagnetic field in the atmospheric surface layer (Holzer 1972). Adushkin and Soloviev (1988) have observed the variations of vertical electric field during the surface detonation of HE with mass 1 t. The amplitude of electric field reached several tens kV/m at the distance 1 km from the explosion site. As the cratering explosion is performed in the medium-moisture rock, the electric signals, as a rule, have a bipolar shape and the polarization of the first phase is negative if z axis is downward directed (Adushkin and Soloviev 1996). This negative phase is usually observed during the course of ground dome development and over the period of ballistic flying of fractured rock fragments. The next more durable phase of the electric field evolution is due to the relaxation of electric charges and the motion of the gas-dust cloud. The duration of this phase is on the order of precipitation time of charged particles and aerosols.

The observed low frequency electric field is believed to be due to the ionization of gas and explosion products as well as from the electrification of fractured rock and soil fragments. In the theory by Adushkin et al. (1990) the gas-dust cloud is modeled by a uniformly charged column filled by detonation products. At first, the negatively charged ground fragments are assumed to be located at the top of the cloud. The kinematic characteristics of the model were chosen in such a way to fit the numerical calculation of the dust cloud evolution with the filming of surface explosion. The ground fragments fall with gravity acceleration, while the precipitation of the small dust particles is described by the following equation:

$$\frac{d\mathbf{v}}{dt} = \mathbf{g} - \frac{\mathbf{V} - \mathbf{V}_g}{\tau} + \frac{q\mathbf{E}}{m}, \tag{11.31}$$

where $\mathbf{g}$ is the free fall acceleration, $\mathbf{V}$ is the speed of descent of the dust particles, $\mathbf{V}_g$ is gas velocity, η is the air viscosity, and m, q, and a stand for average mass, charge, and size of particles, respectively. In the case of laminar flow the relaxation time is given by $\tau = m/(6\pi\eta a)$. Here $\mathbf{E}$ is the sum of geoelectric field and self-consistent field generated by the charged particles in the air and by induced charges on the ground surface. Assuming for the moment that the electric field is close to the breakdown threshold in the air, that is $E = 32\,\mathrm{kV/m}$, and taking the numerical parameters $a = 20$–$50\,\mu\mathrm{m}$, $q = 100e$ (e is elementary charge), we obtain that $qE/m \approx 0.7$–$1.8\,\mathrm{m/s^2} \ll g$. In practice this means that the electric field can be neglected as compared to the gravity.

Figure 11.9 displays the results of numerical calculation shown with dotted line 1 and the experimental observation of vertical electric field generated by a cratering explosion with HE mass 23.8 g (line 2). To fit the numerical and experimental data, the maximal charge of the dust cloud and the height of the cloud lift are estimated as $1.84\,\mu\mathrm{C}$ and 4.2 m, respectively. In making the plot of E_z the following parameters were used $\eta = 1.7 \times 10^{-5}\,\mathrm{Pa \cdot s}$, $a = 48\,\mu\mathrm{m}$. It should be noted that the shape of initial half-wave essentially depends on the charge distribution in the ground dome and in the gas-dust cloud. The sharp spike in the beginning of the second half-wave (dotted line 1) is based on the assumption that all the rock fragments begin to fall simultaneously. As is seen from Fig. 11.9, the experimental data is qualitatively consistent with the simple model presented above. So, the quasi-static electric field caused by the excavating explosion is most likely to be due to the motion of electric charges located in the ground dome and gas-dust cloud.

One more example of transient electric fields detected during a powerful surface explosion with mass 500 t is displayed in Fig. 11.10 (Soloviev and Surkov 2000). The seismic wave arrival at the ground-based station has not a visible effect on the electric field, and the reason may be that the signal was below the sensor sensitivity. The vertical electric field at the distance 1.5 km (line a) reaches a peak value about 2.5 kV/m at the moment $t = 40\,\mathrm{s}$. The numerical calculation shown with line c is based on the simple model of gas-dust cloud which consists of the spherically symmetric charge q_1 situated at the altitude h_1 over the ground and the uniformly charged column with total charge q_2 and altitude h_2. The best fit of the calculated

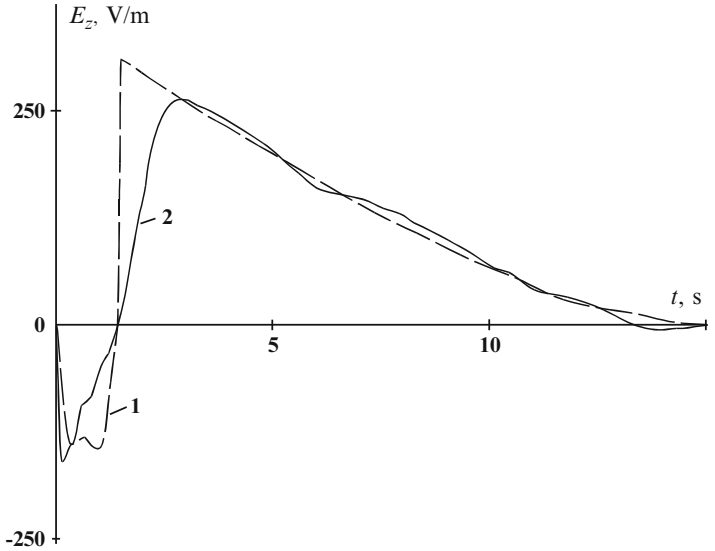

Fig. 11.9 Vertical electric field arising in the surface atmospheric layer under a cratering explosion of HE with mass 23.8 g. The explosion was performed at normalized depth 0.68 m/kg$^{1/3}$. *1*—theoretical calculations, *2*—measurements at distance 5.2 m from the explosion site. Adapted from Adushkin et al. (1990)

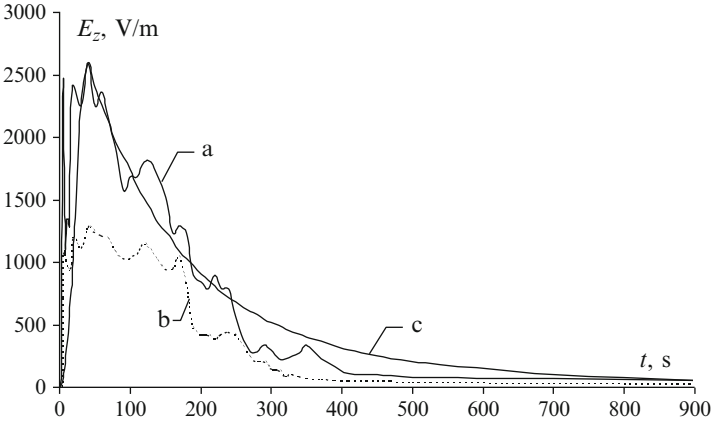

Fig. 11.10 Variations of vertical electric field caused by the HE explosion with mass 500 t as observed at different distances R from the explosion site (Soloviev and Surkov 2000). (**a**) R = 1.5 km; (**b**) R = 2 km; (**c**) R = 1.5 km (model calculation)

and experimental data at the moment 40 s corresponds to the following parameters: $q_1 = 1.3 \pm 0.1$ C, $h_1 = 1.39 \pm 0.06$ km, $q_2 = -0.4 \pm 0.1$C, and $h_2 = 0.30 \pm 0.06$ km.

A series of surface detonations of HE charges with mass of a few kilograms were carried out by Soloviev et al. (2002). The study showed that the amplitude of the

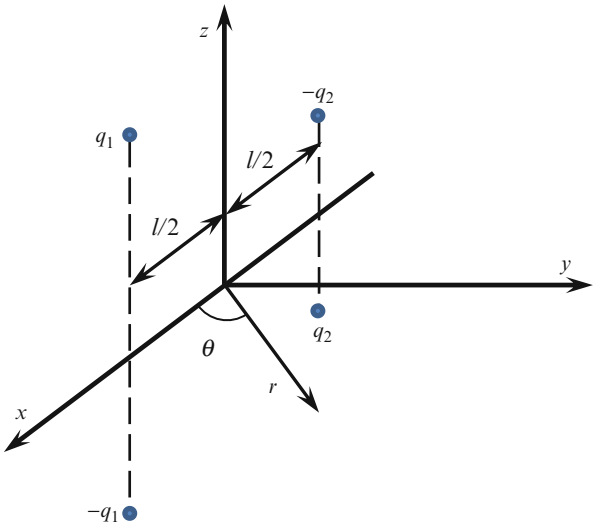

Fig. 11.11 A coordinate system and effective point charges which model the actual charge distribution

electric variations decreases with distance, r, approximately as r^{-4}, at least at the initial stage of the surface explosion. This is indicative of high symmetry of the electric charge distribution which results in a quadrupole character of the electric field in the initial stages of the explosion. In order to interpret the experimental data, the actual charge distribution was modeled by two effective point charges q_1 and $-q_2$ and their mirror images in the conducting ground. The origin of coordinate system is placed at the detonation site while the point charges are located on x, z plane as shown in Fig. 11.11. Far away from the charges the electric field might be expanded in a series of a small parameter l/r where l denotes the distance between the charges. The vertical electric field on the ground surface is given by

$$E_z(r, \theta, t) = -\frac{d_z(t)}{4\pi\varepsilon_0 r^3} - \frac{Q_{xz}(t)}{4\pi\varepsilon_0 r^4} + \ldots \tag{11.32}$$

Here, $d_z = 2(q_1 h_1 - q_2 h_2)$ is the projection of the dipole moment onto the z-axis, and $Q_{xz} = 3l(q_1 h_1 + q_2 h_2)\cos\theta$ is the single nonzero component of the tensor of quadrupole moment of the charge system.

The experimental data suggest that the second term on the right-hand side of Eq. (11.32) is greater than the first one during the initial stage. For the detonation of HE with mass of 5 kg the numerical value $Q_{xz} = -(0.4\text{–}1.3) \times 10^{-4}\,\mathrm{C \cdot m^2}$ brings the closest fit with experimental data. Taking the notice of empirical dependence, according to which the electric charge of products of the surface explosion varies as the 0.65 ± 0.05 power of the explosive mass (Adushkin and Soloviev 1996), the effective charges and the characteristic horizontal distance between them were estimated as $q_1 \approx q_2 \approx 2\,\mu\mathrm{C}$ and 2–7 mm, respectively (Soloviev et al. 2002). It is plausible that the horizontal separation of positive and negative charges in space will

behave randomly. Effective charges may rotate around the vertical axis because of vortices arising beyond the shock front.

The dipole and quadrupole terms in Eq. (11.32) were comparable in some experiments. In the case of explosives with mass of 50 kg the dipole term begins to be prevalent over the quadrupole one at the distances larger than 57 m. It is not surprising because the dipole term decreases more slowly away from the epicenter. So the quadrupole law r^{-4} is applicable in the near zone of explosions which is limited by some critical radius $r_0 = |Q_{xz}/d_z| \sim l\,(q_1h_1 + q_2h_2)\,/\,(q_1h_1 - q_2h_2)$. In the area $r > r_0$ the dipole term predominates and the field amplitude decreases as r^{-3}. It is usually the case that the vertical separation of electric charges and dipole moment increases with time at least when the time is greater than 1–10 s (Adushkin and Soloviev 1996). This implies that the critical distance r_0 decreases with time.

The nuclear explosions are frequently accompanied by the generation of lightning discharges. The five upward-propagating discharges were detected during a thermonuclear detonation "Mike" test with TNT equivalent 10.4 Mt (Uman et al. 1972). The detonation was in the large ground-based hall at Eniwetok Atoll in the Pacific on 31 October 1952. It appears that the lightning discharges were initiated from instrumentation stations slightly above sea level. The major cause of the electric field generation is believed to be the flux of Compton electrons produced by nuclear detonations. For the detonation with such a TNT equivalent the estimated initial number density of ionized particles reaches the value about 10^{15} pair/cm^3, which is sufficient for electrical breakdown in the ionized air (Uman et al. 1972). Laboratory tests and numerical simulations showed that the breakdown conditions, branching and configuration of the discharge channels are determined by the spatial charge distribution in the exposed atmosphere (Hill 1973; Grover 1981; Colvin et al. 1987; Williams et al. 1988).

For the powerful surface explosions the strong quasistatic electric fields can be interpreted in terms of a vortex ring of the heated gas and dust. The lifting of the vortex ring in the atmosphere is caused by Archimedian force which results in the electric charge separation between the vortex ring and dust column. Holzer (1972) has observed an enhancement of the Earth electric field by as much as 60 V/m for the time of the vortex lifting in the atmosphere (2–3 min). The numerical calculations have shown that the electric field at the top of the dust column can reach the breakdown level in the air as the column height increases up to 1–2 km (Surkov 2000). It appears that the lightning can be initiated in the dust cloud of explosion similar to that occurring in the volcanic ash cloud. The IC lightning discharges can explain the sharp peaks which are occasionally observed at the background of quasistatic electric field produced by explosions (Soloviev and Surkov 2000).

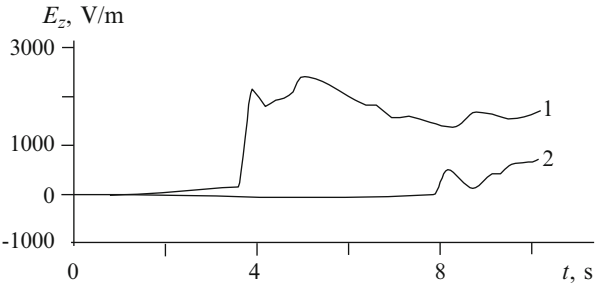

Fig. 11.12 Electric signals caused by aerial wave propagation in the surface atmospheric layer. The signals were measured at the distances (*1*) 1.5 km and (*2*) 2.8 km from the detonation of HE with mass 500 t (Soloviev and Surkov 1994)

11.2.4 Effect of Aerial SWs Propagating in a Surface Atmospheric Layer

A sharp narrow spike in the initial portion of signal shown in Fig. 11.10 took place several seconds after the detonation at the moment of aerial SW arrival at the ground-based station. The electric perturbations caused by the seismic wave propagating in a conductive ground are lower than this spike because the amplitude of seismo-induced effect at the distance $1.5 = 2$ km is about several μV/m (Chaps. 7 and 8). Figure 11.12 illustrates the initial portion of the signals measured at the distances (1) 1.5 km and (2) 2.8 km from the detonation site (Soloviev and Surkov 1994). As is seen from this figure, the front of geoelectric field perturbation approximately propagates at the velocity of aerial wave. So, one may expect that the source of electric variations is the local changes of pressure in the aerial SW.

Almost without exceptions the atmospheric air contains the heavy ions and aerosols which may be both the neutrals and also the charged particles (e.g., see Chalmers 1967; Wåhlin 1986; Sorokin 2007). It is common that the spatial electric charge in the surface atmospheric layer is about 10–500 pC/m^3. Taking into account that the total number density of the heavy ions is on the order of $5 \cdot 10^5 - 10\ \mathrm{m}^{-3}$, the heavy ion excess is estimated as 10^8–$10^9\ \mathrm{m}^{-3}$. Hence the perturbations of the geoelectric field are induced by the changes in the spatial electric charge which is formed by the heavy ions and charged aerosols.

The heavy ions play a crucial role in the formation of the atmospheric electrode layer. However the aerosol particle may greatly affect the electrical parameters of the atmosphere such as the composition and number density of heavy ions and the structure of electrode layer. For the particles with size 0.01–0.2 μm the aerosol number density is about 10^9–$10^{10}\ \mathrm{m}^{-3}$ in rural areas and 10^{10}–$10^{11}\ \mathrm{m}^{-3}$ near towns. The enhancement of the aerosol density gives rise to an increase of the electrode layer depth. Numerical simulations have shown that this depth can vary within 1–100 m by the action of turbulent stirring of the air near the ground surface (Hoppel 1967).

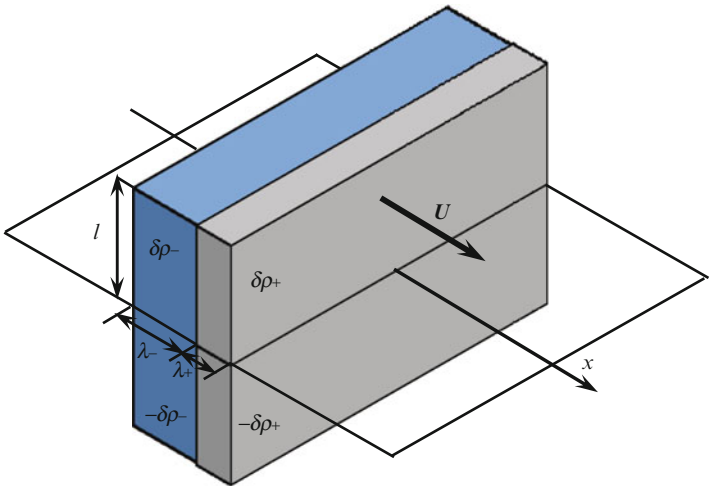

Fig. 11.13 A model of electrical effect caused by an aerial SW propagating in the surface/electrode layer with width l. The charge density variations due to the presence of heavy ions and aerosols are modeled by a step-function. Also shown are the electrical images of the atmospheric charges in the conducting ground

To estimate the aerial SW effect in the electrode layer, we now consider a simple model in which a plane steady SW propagates at constant velocity U along the x axis parallel to the ground surface. The dynamics of the particles motion behind the SW is described by Eq. (11.31). The numerical estimate has shown that the relaxation time $\tau = m/(6\pi\eta a)$, which enter Eq. (11.31), is much smaller than the wave duration. This implies that there will be complete entrainment of aerosols and heavy ions with air flow. In the first approximation the changes in the spatial charge density is supposed to follow the changes in the air density. We set the profile of the gas mass velocity as a rectangular pulse with positive polarity followed by the next one with negative polarity. The amplitudes, V_+ and V_-, and lengths, λ_+ and λ_-, of these rectangular pulses are connected through $V_+\lambda_+ = V_-\lambda_-$. The continuity equation for the electric charge flowing through the SW front is given by

$$\rho_0 U = \rho_+ (U - V_+), \tag{11.33}$$

where ρ_+ denotes the charge density in the air compressed by the SW while ρ_0 is the undisturbed charge density. Hence the small perturbations of the charge density can be written as $\delta\rho_+ = \rho_+ V_+/U$. The charge variations behind the SW front is described by a step-function in such a way that $\delta\rho = \delta\rho_+$ within the length λ_+ of "positive half-wave" and $\delta\rho = \delta\rho_-$ within the length λ_- of "negative half-wave." The model distribution of the charges and their electrical images in the conducting ground is sketched in Fig. 11.13.

If the typical length λ_+ of the aerial wave is much smaller than the width l of the electrode layer, then the model is reduced to the field of a charged thin lateral strip and its electrical mirror image in the conducting ground. In this case we get the following simple estimate of the electric field amplitude on the ground surface

$$E_{\max} \approx \frac{\rho_0 \lambda_+ V_+ \ln(l/\lambda_+)}{\varepsilon_0 U}. \tag{11.34}$$

In the inverse extreme case when $\lambda_+ \gg l$, the problem is reduced to the field of a plane condenser generated by the charges of the atmospheric electrode layer, which is pressed by the SW, and the opposite charges induced in the ground. The solution of this simplified problem is given by

$$E_{\max} \approx \rho_0 l V_+ / (\varepsilon_0 U). \tag{11.35}$$

It should be noted that the exact solution of the problem derived by Soloviev and Surkov (1994) on the basis of Maxwell equations and Eq. (11.31) can be reduced to Eqs. (11.34) and (11.35) in the above extreme cases.

It follows from the observations that the amplitude of the electric field variations is approximately proportional to the parameter $\lambda_+ V_+$ and this tendency keeps for different normalized distances and masses of explosives. It appears that the case of short aerial wave ($\lambda_+ \ll l$) occurs in practice. Substituting the following numerical values $\rho_0 = 8$–$80\,\mathrm{nC/m^3}$, $\lambda_+ = 10\,\mathrm{m}$, $V_+ = 35\,\mathrm{m/s}$, $U = 350\,\mathrm{m/s}$ and $l = 10^2\,\mathrm{m}$ into Eq. (11.34) we obtain $E_{\max} = 0.2$–$2\,\mathrm{kV/m}$. Both this estimate and experimental data shown in Fig. 11.12 are found to be of the same order. It should be noted that the shock compression may result in the release of ions which are in bound state. This leads to the enhancement of the charge density in the SW which results in the increase of the electric field amplitude.

11.2.5 Ionospheric and Magnetospheric Effects

As noted in Chap. 10, the aerial waves is the most efficient way to transfer the energy from the EQs and strong explosions to the ionosphere.

When the aerial SW enters the ionosphere, the entrainment of the ionospheric plasma with neutral flow results in the generation of ionospheric currents and local perturbations of the Earth magnetic field. One of the pioneering studies possibly related to the excitation of the ionosphere by SWs was the variations of the geomagnetic field observed at Irkutsk magnetic observatory after the detonation of Tunguska meteorite in 1908 (e.g., see Ivanov 1961). The abnormal behavior of the geomagnetic field has been observed 2.3 min after the detonation and lasted for several hours.

Considerable attention has been paid in the past to the study of man-made excitation of the ionosphere by the SWs produced by atmospheric nuclear

explosions (Daniels et al. 1960; Lawrie et al. 1961; Stoffregen 1962, 1972; Gassmann 1963; Kotadia 1967; Breitling et al. 1967; Baker and Davies 1968; Baker and Cotten 1971; Kanellakos and Nelson 1972; Lomax and Nielson 1972), surface (Barry et al. 1966; Najita et al. 1975) and underground nuclear explosions (Blanc 1984, 1985; Pokhotelov et al. 1995). SW-induced oscillations in the lower thermosphere followed by the ionospheric perturbations have been observed after a 5 kt chemical explosion (Jacobson et al. 1988). Among the other sources of the strong acoustic waves in the atmosphere and ionosphere are volcano eruptions, spacing flights of supersonic airplanes (Marcos 1966) and rocket launch (Rao 1972; Karlov et al. 1980).

In standard geophysical practice the techniques of vertical, oblique, and Doppler sounding are used in order to examine the ionospheric response to natural and anthropogenic forcing on the Earth's ionosphere. In addition, the technique of continuous VLF electromagnetic transmission probing of the Earth-ionosphere waveguide is in routine use (e.g., see Surkov 2000; Molchanov and Hayakawa 2008). The experimental evidences on the impact of surface and underground explosions on the ionospheric F, E, and D layers have been demonstrated on the basis of these techniques (e.g., see Barry et al. 1966; Broche 1977; Blanc 1984, 1985). In the epicentral region the effect of explosion on the ionosphere is predominantly due to the upward-propagating atmospheric acoustic wave. This wave is generated when the underground SW reflects from the ground surface. The amplitude of mass velocity in the aerial wave increases with altitude due to the exponential fall off of the atmospheric density. Even a weak upward propagating wave can be converted into an SW because of nonlinear properties of the atmosphere. This nonlinear transformation of the wave shape and wave-front breaking occurs at the altitude $H_* \approx 2P_0/\left(\rho_g g\right) \sim 20\,\mathrm{km}$ where P_0 and ρ_g are the pressure and air density at the sea level (e.g., see Whitham 1974). As the altitude is larger than H_*, the wave profile becomes universal. The wave front has a triangular shape. It is imperative that the compression phase is followed by the rarefaction phase in such a way that the wave profile resembles a letter N, as shown in Fig. 11.13. It follows from the principle of conservation of momentum that the positive and negative phases of the N-wave are equal in square (e.g., Landau and Lifshitz 1959). In the bottom of the ionosphere; that is, in the altitude range of 90–100 km, the amplitude of mass velocity and length of the N-wave can reach several tens m/s and several km, respectively. The exponential increase of the SW amplitude ceases at the altitudes over 100 km. The cause of this effect is the enhancement of the gas viscosity at these altitudes due to the increase of mean free path of molecules (Enstrom et al. 1972). Then the dissipative processes result in both the decrease in the pressure and mass velocity gradients at the SW front and the increase in the wavelength which can reach a few tens km in F-region of the ionosphere.

The numerical stimulations have shown that the effect of SW impact on the lower ionosphere is maximal in the circular area with radius of the order of 100 km (Orlov and Uralov 1984), and the influence of shock upon the ionosphere diminishes essentially outside this area. This effect is due to the refraction of sound in the

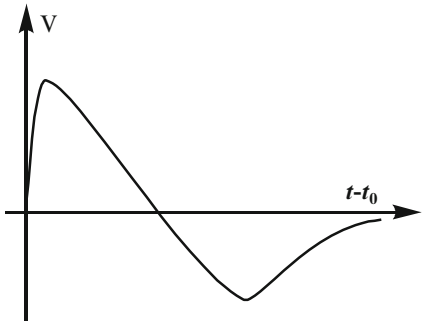

Fig. 11.14 Mass velocity of gas in the atmospheric acoustic wave at high altitudes versus time. Here t_0 is a moment of SW front arrival at given point

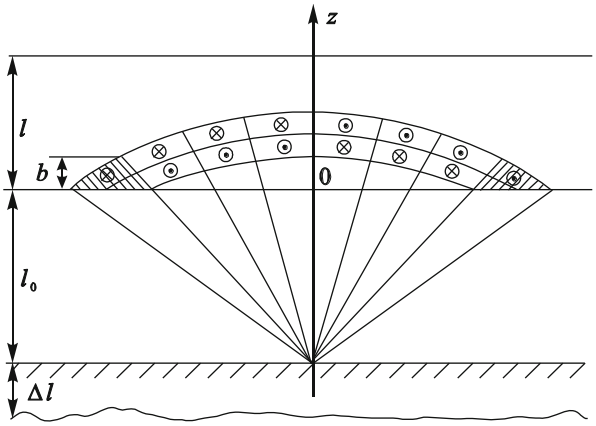

Fig. 11.15 A model of the atmosphere ($-l_0 < z < 0$) and the ionospheric E-layer ($0 < z < l$). An aerial SW is originated from the source/explosion located on the ground surface $z = -l_0$. A bundle of direct lines represents the directions of SW propagation. The circles with crosses and points in the middle show the opposite directions for wind-driven/extrinsic currents. These currents were not compensated in the shaded region of the ionosphere. A polygonal line at the bottom of this figure shows a depth Δl of the layer of sedimentary rocks which have a high conductivity

stratosphere and thermosphere which results in the sound ray curvature and rotation down to the earth.

In what follows we study the ionospheric perturbations caused by the axially symmetrical SW propagating from the explosion site situated at the ground surface towards the ionosphere. The mass velocity has a contour of "N-wave" which is shown in Fig. 11.14. We use the plane-stratified model of the medium which consists of the conducting ground ($z < -l_0$), the nonconducting atmosphere ($-l_0 < z < 0$) and gyrotropic E-layer of the ionosphere ($0 < z < l$). The origin of coordinate system is placed on the symmetry axis of the wave at the lower boundary of the ionosphere. In Fig. 11.15 the bundle of direct lines sketches the directions of SW propagation from the explosion site. In this region the acoustic wave refraction is ignored.

To study the ionospheric perturbations in a little more detail we consider first a polar ionosphere. The geomagnetic field $\mathbf{B}_0$ is therefore vertically parallel to z axis. In this case Maxwell equations in the ionospheric E-layer can be written in cylindrical coordinates

$$-\partial_z B_\varphi = \mu_0 \left(\sigma_P E_r - \sigma_H E_\varphi + \sigma_H V_r B_0\right), \tag{11.36}$$

$$\partial_z B_r - \partial_r B_z = \mu_0 \left(\sigma_P E_\varphi + \sigma_H E_r - \sigma_P V_r B_0\right), \tag{11.37}$$

$$r^{-1}\partial_r \left(r B_r\right) + \partial_z B_z = 0, \tag{11.38}$$

where B_z, B_r, and B_φ are the components of the geomagnetic field perturbations, E_r and E_φ are the components of the electric perturbations. Pedersen and Hall conductivities of the ionospheric plasma, i.e. σ_P and σ_H, are considered as constant values. The field-aligned ionospheric conductivity is assumed to be infinite and hence $E_z = 0$. At given orientation of the vector $\mathbf{B}_0$, only radial component V_r of the gas velocity enters the set of Eqs. (11.36)–(11.38).

The area of gas flow due to the acoustic wave is shown in Fig. 11.15 with three arcs. This area is of a form of narrow band since the longitudinal size of the acoustic wave is much smaller than a width l of the ionospheric E region. The upper arc corresponds to the N-wave front. Because of the bipolar form of the acoustic N-wave, at first the gas moves forward in radial directions and then it moves back. The first area is bounded by the upper and middle arcs, while the next area is restricted by the middle and lower arcs. The currents generated by the motion of conductive media are oppositely directed in these areas. The changes in the current direction occur in the middle portion of the wave where the gas velocity vanishes. In Fig. 11.15 the opposite directions of the extrinsic currents are represented by the circles with cross and point.

The total extrinsic current is proportional to the integral of the gas velocity over the area covered by the wave. Now we divide this area into narrow sectors in the z, r plane formed by rays diverging from the explosion point. Notice that the currents flowing through the upper and lower portions of these sectors are oppositely directed. The total current of each sector is proportional to the integral of the gas velocity along the corresponding ray. For N-wave this integral is equal to zero, so that the corresponding extrinsic current vanishes as well. As is seen from Fig. 11.15, only the last shaded cells on the right and on the left contain the unbalanced currents. Certainly, this approach is valid for the short N-waves. Usually the longitudinal size of the acoustic waves $b \approx 1-3$ km while the width of the E-layer is about 20–30 km so that the condition $b \ll l$ is true.

Thus, the uncompensated extrinsic current arises only at the lower boundary of the ionosphere. The cross section of this ring current is on the order of the longitudinal wave size. This implies that the extrinsic current density is nonzero only inside the narrow layer $b \ll l$ in the vicinity of the ionosphere bottom, that is at $z = 0$. To simplify the problem, we formally assume that the velocity altitude distribution is described by a delta-function, that is $V_r = b\delta(z)\, V_r(r, t)$. Performing

integration of Eqs. (11.36) and (11.37) over z from zero to ε and then assuming $\varepsilon \to 0$ we come to the following boundary conditions at $z = 0$

$$B_{\varphi a} - B_{\varphi i} = \mu_0 b J_H, \quad B_{ra} - B_{ri} = \mu_0 b J_P, \quad B_{za} = B_{zi}, \tag{11.39}$$

where the subscripts a and i are related to the atmosphere and ionosphere, respectively. The extrinsic current densities, $J_H = \sigma_H V_r B_0$ and $J_P = \sigma_P V_r B_0$, are assumed to be given functions.

Equations (11.36) and (11.37) can be solved for E_r and E_φ. Substituting these components of electric field into Maxwell equation $\nabla \times \mathbf{E} = -\partial_t \mathbf{B}$ and rearranging yields

$$\partial_t B_z = D_P \nabla^2 B_z - \frac{D_H}{r} \partial_r \left(r \partial_z B_\varphi \right), \tag{11.40}$$

$$\partial_t B_r = D_P \left(\nabla^2 B_r - \frac{B_r}{r^2} \right) + D_H \partial_{zz}^2 B_\varphi, \tag{11.41}$$

$$\partial_t B_\varphi = D_P \nabla^2 B_\varphi - D_H \left(\nabla^2 B_r - \frac{B_r}{r^2} \right), \tag{11.42}$$

where

$$D_P = \frac{\sigma_P}{\mu_0 \left(\sigma_P^2 + \sigma_H^2 \right)}, \quad D_H = \frac{\sigma_H}{\mu_0 \left(\sigma_P^2 + \sigma_H^2 \right)}, \tag{11.43}$$

are the coefficients of diffusion in a gyrotropic medium and the operator ∇^2 is given by

$$\nabla^2 = r^{-1} \partial_r + \partial_{rr}^2 + \partial_{zz}^2. \tag{11.44}$$

The set of Eqs. (11.40)–(11.42) can be solved with respect to each component of the magnetic perturbation. For example, excluding B_φ from Eq. (11.40) gives (Surkov 1996)

$$\partial_t \left(\partial_t B_z - D_P \nabla^2 B_z \right) = \partial_{zz}^2 \left\{ D_p \partial_t B_z - \left(D_P^2 + D_H^2 \right) \left(\nabla^2 B_z - B_z / r^2 \right) \right\}. \tag{11.45}$$

Applying Eq. (11.36) to the atmosphere and taking into account that the components of the conductivity tensor are equal to zero, we obtain that $B_\varphi = 0$ everywhere in the atmosphere. Other components of the GMP can be determined from the Laplace equation:

$$\nabla^2 B_r = B_r / r^2, \quad \nabla^2 B_z = 0. \tag{11.46}$$

Suppose that the acoustic wave reaches the lower boundary of the ionosphere at the moment $t = 0$. The region of interaction between the wave and ionosphere

increases in time, but we shall assume the simultaneous arrival of waves at the ionospheric boundary. Owing to the wave refraction in the atmosphere, the ionospheric region interacting with the wave is limited by the radius $a \sim l_0 \approx 100$ km. As alluded to earlier in Chap. 7, the GMP will propagate into the ionosphere in accordance with the diffusion law. For the time t the diffusion front climbs to the altitude $z_d \sim 2\left\{t/\left(\mu_0\sigma_p\right)\right\}^{1/2}$ and thus the front will reach the upper boundary of the ionospheric E-layer at the moment $t_d \sim \mu_0\sigma_p l^2/4$. In what follows we restrict our study to the short interval $0 < t < t_d$ which corresponds to the initial stage of signal. During this interval the solution of Eqs. (11.40)–(11.42) weakly depends on the boundary conditions of the problem at $z = l$. Hence, we replace this condition by the requirement that the solution must be finite when $z \to \infty$.

Considering the GMP diffusion in a horizontal direction, we note that for the time $t < t_d$ the diffusion front propagates at the distance much smaller than a. So, we will neglect the lateral expansion of the diffusion region in the ionosphere and focus on the vertical propagation of the GMP. This implies that in the region $r < a$ the terms $\partial_{rr}^2 B_z$, $r^{-1}\partial_r B_z$, and B_z/r^2 in Eq. (11.45) are much smaller than $\partial_{zz}^2 B_z$. As a first approximation, we assume that B_z is not a function of r. Notice that the components B_r and B_φ are equal to zero at $r = 0$ and their dependence on r should already be taken into account in the first approximation.

Laplace transformation with respect to time can be applied to all the equations with boundary conditions. Let b_z, b_r, b_φ, and j be Laplace transforms of the magnetic perturbations and extrinsic current density, respectively. Taking the notice of the above approximations, one can reduce Eq. (11.45) to the following:

$$\frac{d^4 b_z}{dz^4} - 2p\mu_0\sigma_P \frac{d^2 b_z}{dz^2} + p^2\mu_0^2\left(\sigma_P^2 + \sigma_H^2\right) b_z = 0, \tag{11.47}$$

where p denotes the parameter of Laplace transformation. When the finiteness of b_z at $z \to \infty$ is taken into account, the solution of (11.47) is given by

$$b_{zi} = C_1 \exp\left(-\lambda_+ z\right) + C_2 \exp\left(-\lambda_- z\right); \quad \lambda_\pm = \left\{\mu_0 p\left(\sigma_P \pm i\sigma_H\right)\right\}^{1/2}, \tag{11.48}$$

where C_1 and C_2 are the arbitrary constants, and $\mathrm{Re}\lambda_\pm > 0$. Other components of the magnetic perturbations in the ionosphere can be expressed through b_{zi} via

$$b_{ri} = -\frac{1}{r}\int_0^r r' \frac{db_{zi}}{dz} dr', \tag{11.49}$$

$$b_{\varphi i} = -\frac{1}{r}\int_0^r r' \left\{\frac{1}{p\mu_0\sigma_H}\frac{d^3 b_{zi}}{dz^3} - \frac{\sigma_P}{\sigma_H}\frac{db_{zi}}{dz}\right\} dr', \tag{11.50}$$

In the same approximation the equation for the atmosphere ($-l_0 < z < 0$) reads: $d^2 b_z / dz^2 = 0$. If the ground is considered as a perfect conductor, the solution of this equation is given by

$$b_{za} = C_0 (z + l_0). \tag{11.51}$$

The arbitrary constants C_0, C_1, and C_2 can be found from Eqs. (11.48)–(11.51) and the boundary conditions given by Eq. (11.39).

Now consider the low frequency perturbations when the corresponding skin-depth in the ground is greater than the depth $\Delta l \approx$ 1–2 km of upper layer of sedimentary rocks which possess a high conductivity. The lower boundary of the sedimentary rock layer is shown in Fig. 11.15 with wavy line. In this extreme case we can consider this layer as if it were transparent for the GMP. To simplify the problem, we assume that formally l_0 goes to infinity. Then the inverse Laplace transformation of the solution can be reduced to the simple quadratures. For example, in the ionosphere ($z \geq 0$) the result can be written as follows (Surkov 1996)

$$B_{zi}(z, r, t) = -b \left(\frac{\mu_0}{2\pi \sigma_H} \right)^{1/2} r^{-1} \partial_r r \int_0^t G_z (z, t') J_H (r, t - t') \, dt', \tag{11.52}$$

$$B_{\varphi i}(z, r, t) = \frac{\mu_0 z b}{2} \left(\frac{\mu_0 \sigma_H}{2\pi} \right)^{1/2} \int_0^t G_\varphi (z, t') J_H (r, t - t') \, dt', \tag{11.53}$$

where the functions G_z and G_φ are given by

$$G_z = \frac{1}{t^{1/2}} \left(\gamma_+ \cos \frac{\alpha z^2}{t} + \gamma_- \sin \frac{\alpha z^2}{t} \right) \exp \left(-\frac{\beta z^2}{t} \right), \tag{11.54}$$

$$G_\varphi = \frac{1}{t^{3/2}} \left(\chi_+ \sin \frac{\alpha z^2}{t} - \chi_- \cos \frac{\alpha z^2}{t} \right) \exp \left(-\frac{\beta z^2}{t} \right). \tag{11.55}$$

Here the following abbreviations are introduced

$$\chi_\pm = m\gamma_\pm - \gamma_\mp, \quad \gamma_\pm = \left\{ \left(1 + m^2\right)^{1/2} \pm m \right\}^{1/2},$$
$$\alpha = \frac{\mu_0 \sigma_H}{4}, \quad \beta = \frac{\mu_0 \sigma_P}{4}, \quad m = \frac{\sigma_P}{\sigma_H}. \tag{11.56}$$

In order to analyze the features of this solution, we choose the pulsed source as a simple model of extrinsic current, that is $J_H (r, t) = \sigma_H B_0 V_* r \eta (a - r) T \delta (t) / a$, where $\delta (t)$ denotes δ-function, $\eta (a - r)$ is the step-function, V_* is the amplitude of mass velocity at the lower boundary of the ionosphere, and T is the typical time

scale. As is seen from this expression, the extrinsic current flows in the circle with radius a and it vanishes outside this area. In this case the integrals in Eqs. (11.52) and (11.53) can be easily calculated (Surkov 1996)

$$B_{zi} = -\frac{2B_0 V_* bT}{a}\left(\frac{\mu_0\sigma_H}{2\pi}\right)^{1/2} G_z(z,t), \quad B_{ri} = -\frac{r}{2}\partial_z B_{zi}, \tag{11.57}$$

$$B_{\varphi i} = \frac{B_0 V_* bTzr}{a\,(2\pi)^{1/2}}\left(\mu_0\sigma_H\right)^{3/2} G_\varphi(z,t). \tag{11.58}$$

where the functions G_z and G_φ are determined by Eqs. (11.54) and (11.55).

We recall that Eqs. (11.57) and (11.58) are valid in the interval $t < t_d$, which can be applied to the front of electromagnetic perturbations. Formally this solution describes the case of infinite gyrotropic conductive half-space bordering the atmosphere.

The factor $\exp\left\{-\mu_0\sigma_P z^2/(4t)\right\}$ is indicative of the diffusion character of the GMP propagation across the ionospheric E-layer. Danilov and Dovzhenko (1987) have noted that this factor determines the length of an electromagnetic precursor for acoustic wave. This effect is similar to the electromagnetic forerunner of seismic wave that we have examined in more detail in Chap. 7. Substituting σ_p for σ in Eq. (7.20) we obtain the estimate of the precursor length $\lambda \sim (\mu_0\sigma_P C_a)^{-1}$, where C_a is the acoustic wave velocity.

The damping factor in Eqs. (11.54) and (11.55) is analogous to the skin effect in conductive media. However, the oscillating factors in these equations lead to a new property of this effect because the diffusion perturbations propagate in a form of damped oscillation. The phase of the oscillations $\mu_0\sigma_H z^2/(4t)$ depends merely on the Hall conductivity, which means that the effect essentially depends on the presence of magnetized electrons in the ionospheric plasma of the E layer. The oscillation period increases in time and the oscillations cease at $t > \mu_0\sigma_H z^2/(4\pi)$. By analogy with the above line of reasoning, one can estimate the "oscillatory" length of the electromagnetic precursor as $\lambda_o \sim (\mu_0\sigma_H C_a)^{-1}$.

The same regime of diffusion has been demonstrated to be excited in the ionosphere for the case of horizontal geomagnetic field (Surkov 1990a,b). In the Hall medium, the analogous type of micropulsations propagating along the geomagnetic field has been termed the Schrödinger mode (Greifinger and Greifinger 1965). Another way to explain the oscillatory structure of the electromagnetic forerunner in the magnetoactive plasma is to take into account the radiations of helicon waves which are known as whistler mode in the geophysical practice. As the electrons are magnetized whereas the ions are not yet, the dispersion relation for the field-aligned helicons reads (e.g., Lifshitz and Pitaevskii 1981)

$$\omega = \frac{k^2 V_A^2}{\Omega_H} \tag{11.59}$$

where k is the wave number and Ω_H is the ion gyrofrequency. In the coordinate system which moves at the acoustic wave velocity, the dispersion relation is given by (Danilov and Teselkin 1984)

$$\omega' - kC_a = \frac{k^2 V_A^2}{\Omega_H}. \tag{11.60}$$

In the stationary problem under consideration, the frequency $\omega' = 0$ whence it follows the typical size of the precursor is about $\lambda_o \sim k^{-1} = V_A^2/(C_a\Omega_H)$. We recall that these equations are valid if the electrons are magnetized, that is, $\omega_H \gg \nu_e$, and the ions are not yet, that is $\Omega_H \ll \nu_{in}$. Taking into account that in this case $\sigma_H \approx e^2 n/(m_e\omega_H) = en/B_0$ and substituting $\Omega_H = eB_0/\overline{m_i}$ and $V_A^2 = B_0^2/(\mu_0 n\overline{m_i})$ into the above estimate, we obtain the length of "oscillatory" portion of the electromagnetic precursor $\lambda_o \sim (\mu_0\sigma_H C_a)^{-1}$ which coincides with the above estimate.

It appears that a high-power surface detonation can have influence not only on the ionosphere but also on the magnetosphere. For example, the magnetic pulses with amplitude 100 nT have been detected onboard AUREOL-3 satellite at the altitude about 750 km several minutes after the surface detonation known as experiment MASSA-1 (Galperin and Hayakawa 1996). The detonation of HE with TNT equivalent 288 t has been performed in a sandy desert 60 km to the north of Alma-Ata (former USSR) on November 28, 1981. In order to discuss the plausibility of the coupling mechanisms operating between the surface detonation and the magnetosphere, it is necessary at this point to estimate the magnitude of the signals produced by the surface detonation at the magnetospheric altitudes. To do this, we suppose that Eqs. (11.40)–(11.42) are justified in the altitude range $0 < z < l$ while above this layer; that is at $z > l$, there take place the equations for a cold collisionless plasma. Assuming that the field-aligned plasma conductivity is infinite, we come to the standard equations describing Alfvén and FMS plasma waves in this region

$$\partial_{tt}^2 B_z = V_A^2 \nabla^2 B_z, \quad \partial_{tt}^2 B_\varphi = V_A^2 \partial_{zz}^2 B_\varphi. \tag{11.61}$$

where V_A is the Alfvén wave speed. Disregarding, as before, the derivatives of r in the operator ∇^2, we choose the solution of Eq. (11.61) in a form of upgoing waves. The proper boundary condition at $z = l$ is that the solution would transform continuously into that of Eqs. (11.40)–(11.42).

It is easy to show that the solution of Eq. (11.61) appears as Eqs. (11.57)–(11.58) where z and t should be replaced by l and $\tau = t - (z-l)/V_A$, respectively. This means that the same temporal dependence holds if we use the coordinate system which moves at the Alfvén wave velocity. The components B_z, B_r, and E_φ describe Alfvén wave, while the components E_r, E_z, and B_φ correspond to FMS wave. The numerical modeling of the GMP in the magnetosphere versus τ is displayed in Fig. 11.16. Here we made use of Eqs. (11.57)–(11.58) and the typical parameters

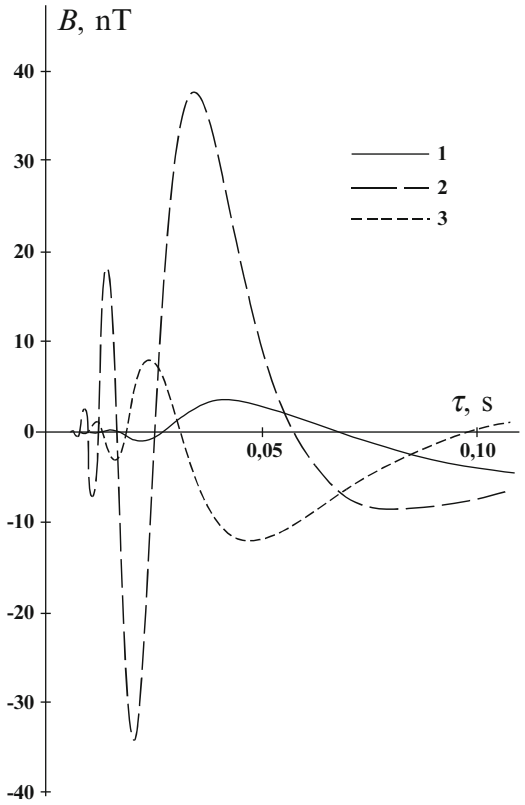

Fig. 11.16 Numerical simulation of magnetic perturbations in the polar magnetosphere. The extrinsic current at the lower boundary of the ionosphere is modeled by the delta-function of time. The components B_z, B_r, and B_φ versus $\tau = t-(z-l)/V_A$ are shown with lines 1, 2, and 3, respectively (Surkov 1996)

of the dayside ionospheric E-layer; that is, $\sigma_P = 0.5\sigma_H = 2.5 \cdot 10^{-4}$ S/m, $V_A = 300$ km/s as well as the following numerical values $b = 3$ km, $a = 100$ km, $r = 90$ km, $T = 0.1$ s.

Next consider the case when the source function/extrinsic current is modeled by a step function of time, that is $J_H(r,t) = \sigma_H B_0 V_* r \eta(a-r)\, T\eta(t)/a$. In this case the integrals in Eqs. (11.52) and (11.53) are not expressed by the elementary functions though the component B_r can be written as

$$B_{ri} = -\frac{B_0 V_* br}{aV_A}\left(\frac{\mu_0\sigma_H}{2\pi}\right)^{1/2} G_z(l,\tau). \tag{11.62}$$

For this extreme case the results of numerical calculations are shown in Fig. 11.17.

As is seen from Figs. 11.16 and 11.17, the risetime of the signals is approximately coincident with that of the exponential factor $\exp\left\{-\mu_0\sigma_P l^2/(4\tau)\right\}$. This time is of the order of diffusion time through the conducting E-layer $t_d \sim \mu_0\sigma_P l^2/4 \approx 0.07$ s. The oscillations with the phase $\mu_0\sigma_H l^2/(4\tau)$ are due to the Hall conductivity of the ionospheric plasma. The period of oscillations increases in time until they disappear at the moment $t > t_o = \mu_0\sigma_H l^2/4 \approx 0.05$ s. The substitution of the step function

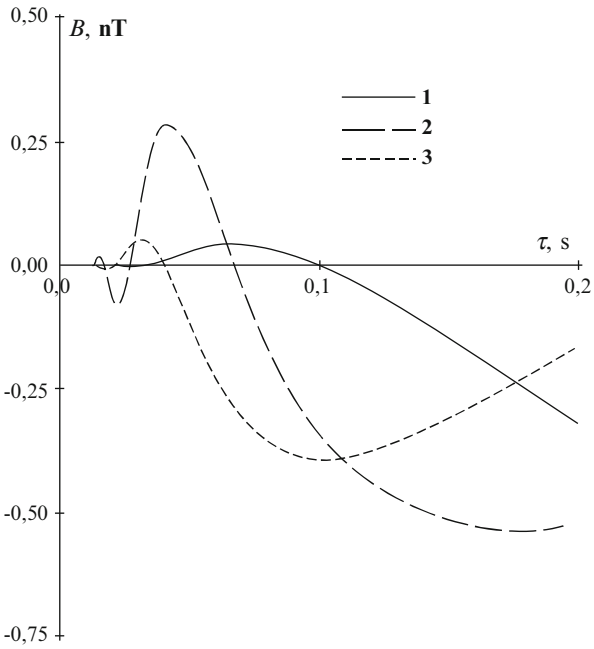

Fig. 11.17 Numerical simulation of magnetic perturbations in the polar magnetosphere. The extrinsic current at the lower boundary of the ionosphere is modeled by the step function of time. The components B_z, B_r, and B_φ versus $\tau = t - (z - l)/V_A$ are shown with lines 1, 2, and 3, respectively (Surkov 1996)

of time in Eqs. (11.52) and (11.53) results in smoothing these oscillations though a few oscillations remain in the initial part of the signal. As we noted above, such a structure is typical of the nonstationary diffusion process in gyrotropic media. In the model of the magnetosphere the wave profile is steady in the reference frame moving at the Alfvén wave velocity. It is not surprising, then, that this structure of perturbations is saved in the Alfvén and FMS waves and hence it is transferred upward at the Alfvén velocity.

It should be noted that the solution at $z > l$ is not entirely correct because the approximation of collisionless plasma is inapplicable to the typical wave frequencies $\nu = 0.1$–1 Hz at the altitudes of F layer. The decrease of the wave amplitude due to energy dissipation in the F layer can be roughly estimated by means of the attenuation factor $\exp\left(-z^2\mu_0\sigma_P\nu/4\right)$. Substituting $\sigma_P = 10^{-5}$ S/m, $z = 200$ km as a mean altitude of the F layer and the above frequencies into this factor gives a decrease of the amplitude at 1.1–3.5 times. Certainly, a strong fall off of the spectrum should be expected in the frequency range above 1 Hz.

The effect of opposite polarity can arise approximately 1–2 min the after acoustic wave arrival at the bottom of the ionosphere when the wave will cross the upper boundary of the E layer. In such a case the area of uncompensated extrinsic current appears at this boundary. This current flows oppositely to direction of the extrinsic current at lower surface of the ionosphere that results in the generation of GMP of the opposite polarity. The amplitude of these GMPs can significantly exceed the original perturbations since the velocity amplitude and the length of the acoustic wave increase with altitude.

As one might expect, the front structure of the Alfvén and FMS waves in the magnetosphere is correlated with the processes in the ionospheric E layer. The front duration is of the order of t_d or t_0 while the typical front length is $V_A t_d$ or $V_A t_0$, that is about 15–20 km at the altitudes of a few hundreds km. The total duration of perturbations is determined by the time of acoustic wave passage through E layer and thus it can be far beyond the duration of the wave front (Surkov 1992a,b). The area of perturbations is extended along the geomagnetic field lines. The lateral size of this area is about 100 km which appear to be much less than the field-aligned scale. The sharp front and gradual drop of the signals shown in Figs. 11.16 and 11.17 are in qualitative agreement with the onboard observations though the predicted amplitudes of the signals (∼0.1–10 nT) are much smaller than that measured by the satellite AUREOL-3 (∼ 100 nT). It should be noted that on a basis of Maxwell equations one can find the following simple estimate of the GMP amplitude (e.g., see Danilov and Dovzhenko 1987)

$$\Delta B \sim \mathrm{Rm} B_0 \Delta p / p, \tag{11.63}$$

where Δp is excess pressure and $\mathrm{Rm} = \mu_0 \sigma_P \lambda V_a$ is magnetic Reynolds number. Taking the numerical values of the wavelength $\lambda = 1$ km and $\Delta p/p = 0.1$ we obtain the value $\Delta B \sim 1$ nT which is in agreement with the satellite observations (Pokhotelov et al. 1995). Certainly these rough estimates essentially depend on the parameters of the ionosphere, diurnal variations, and so on.

The splitting of the perturbations into two types in the lower ionosphere has occasionally been observed under nuclear explosions (Daniels et al. 1960). In the upper ionosphere these vertically traveling perturbations had different velocities. It appears that the slow perturbation corresponded to the conventional sound wave, whereas the velocity of the fast perturbation was increased roughly 2 times. It was hypothesized by Wickersham (1970) that this effect can be due to the excitation of ion-sound mode at the altitude range of 160–200 km. The velocities of the sound C_a and ion-sound V_i waves are given by

$$V_a = \left(\frac{\gamma k_B T}{\overline{m}} \right)^{1/2}, \quad V_i = \left(\frac{k_B \{ Z \gamma_e T_e + \gamma_i T_i \}}{\overline{m_i}} \right)^{1/2}, \tag{11.64}$$

where Z denotes the ion charge; $\overline{m}$ and $\overline{m_i}$ are the average masses of neutrals and ions; γ_e, γ_i and γ stand for adiabatic exponents of the electrons, ions, and neutral gases; and T_e, T_i, and T are their temperatures, respectively. In the theory the ion sound can be generated in a strongly anisothermic plasma ($T_e \gg T_i$) when the frequency of inelastic collisions between the charged and neutral particles exceeds the frequency of their elastic collisions. However in the media of neutral particles the ion sound mode undergoes a strong attenuation because of the collisions between ions and neutrals. In order to overcome this difficulty, one should assume a possibility for some wave-induced exothermic reactions which results in the enhancement of the particle temperature (Wickersham 1970).

The powerful explosions can generate not only acoustic but also internal gravity waves (IGWs) in the atmosphere. It is well known that IGWs develop in media whose density varies with altitude and, in particular, in the stratified media. Basically, these waves propagate horizontally along the Earth surface at the velocities up to 400–500 m/s. At the epicentral distance of 1,200 km the period of IGW is about 7 min while the period of the acoustic wave is approximately equal to 1–2 min (Broche 1977).

The satellite observations have shown the increase of the electric noises in the frequency range of 0.1–1 kHz 6–7 min after the surface detonation MASSA-1 (Galperin and Hayakawa 1996). The enhanced noises were detected within ± 200 km around the magnetoconjugate tube with $L \approx 1.5$. The field-aligned electric components exhibited the greatest noise amplitude while the most spectral intensity is related to the frequency region below 100 Hz. Taking the notice of weak magnetic perturbations in this region, the observed effect is assumed to be the result of electrostatic turbulence induced by Alfvén waves propagating along the magnetoconjugate paths (Pokhotelov et al. 1994). The similar effect has been observed in the vicinity of the magnetoconjugate tube during the experiment MASSA-2 (Galperin and Hayakawa 1996). The region of the electric noise expanded at the velocity about 0.6 km/s up to the altitudes about 10^3 km.

Of interest in the analysis of satellite observations is the strong Alfvén pulses (with amplitudes 117 and 50 nT) measured by AUREOL-3 with onboard magnetometers and electric field sensors several minutes after HE detonations MASSA-1 and MASSA-3. The above estimates have shown that the acoustic channel of the explosion energy transfer to the ionosphere cannot be so effective in order to excite the pulses with so high amplitudes. It has been speculated that this effect can be attributed to the electric discharge generated at the SW front (Galperin and Hayakawa 1996, 1998; Surkov and Galperin 2000). The thermal ionization and changes in constants of chemical and ionization equilibrium can lead to an increase of the conductivity at the SW. In this notation, the SW surface with the enhanced conductivity and the bottom of the ionosphere form a peculiar kind of capacitor which can be charged by chance. For example, as the aerial SW propagates through the thundercloud or dust cloud or the wave flank crosses them, then a portion of the charge can flow from the cloud to the wave surface. Assuming for the moment that the total charge captured from the cloud is about 20 C and considering the SW as a hemisphere with radius of 60 km, the average surface charge density has to be about $0.9\,\mathrm{nC/m^2}$ which corresponds to the electric field $10^2\,\mathrm{V/m}$. This value is close to the air breakdown threshold, 130–250 V/m, at the altitudes 60–70 km. So one might expect the generation of the electric discharges between the SW and the ionosphere such as BJs or so on. It was hypothesized that this kind of discharge can be initiated by a meteor-burst channel of ionization. Certainly, this is only the maximal estimate of the effect because the charge decreases continuously due to the atmospheric conductivity. In addition, the favorable circumstances such as appropriate meteor path are desirable to explain this exotic phenomenon.

Appendix I: Magnetic Perturbations Caused by Underground Detonation

High-Heated Plasma Ball Expanding in Ambient Magnetic Field

Let us consider an expanding homogeneous plasma ball immersed into the uniform magnetic field with induction $\mathbf{B}_0$ (Ablyazov et al. 1988). At the time $t = 0$ the ball radius begins to increase in accordance with the dependence $R(t) = R_0\beta(t)$ where R_0 is the initial ball radius and $\beta(t)$ is a given function, which is equal to unity at $t = 0$. The plasma conductivity obeys the known law $\sigma_p = \sigma_p(t)$ as well. We assume that the plasma ball is surrounded by the non-magnetic rock ($\mu = 1$) whose conductivity is everywhere negligible compared with the plasma one. As the ball is situated at the depth which is much greater than the ball radius, one can neglect the influence of the atmosphere in calculating the field in the vicinity of the ball. In this approach the magnetic induction $\mathbf{B}$ in the plasma ball is described by the quasi-stationary Maxwell equations ($0 < r < R$)

$$\partial_t \mathbf{B} = \nabla \times (\mathbf{V} \times \mathbf{B}) + \frac{1}{\mu_0 \sigma_p} \nabla^2 \mathbf{B}, \qquad \nabla \cdot \mathbf{B} = 0, \tag{11.65}$$

where $\mathbf{V}$ is the plasma velocity.

Since the rock conductivity is ignored, Maxwell equations outside the ball are given by $\nabla \times \mathbf{B} = 0$ and $\nabla \cdot \mathbf{B} = 0$. In this region we seek for the solution of these equations as a sum of the uniform field, $\mathbf{B}_0$, and of the field of effective magnetic dipole whose moment is proportional to $\mathbf{B}_0$. If the origin of spherical coordinate system is placed in the ball center, the solution of the problem can be represented as follows ($r > R$)

$$\mathbf{B} = B_0 \left[\cos\theta \left(\frac{2\chi R_0^3}{r^3} + 1 \right) \hat{\mathbf{r}} + \sin\theta \left(\frac{\chi R_0^3}{r^3} - 1 \right) \hat{\boldsymbol{\theta}} \right], \tag{11.66}$$

where the angle θ is measured from the direction of $\mathbf{B}_0$ and $\hat{\mathbf{r}}$ and $\hat{\boldsymbol{\theta}}$ denote the unit vectors of spherical coordinate system. Here the dimensionless function $\chi(t)$ is related to the magnetic moment of the plasma ball through the following relationship $\mathbf{M}(t) = 4\pi\chi(t) R_0^3 \mathbf{B}_0/\mu_0$.

The plasma ball is assumed to expand uniformly so that the plasma moves in radial directions. Consequently, the radius-vector of an elementary plasma volume can be written as $\mathbf{r} = \mathbf{r}_0\beta(t)$, where $\mathbf{r}_0$ denotes the initial coordinate of the elementary volume. Whence it follows that the plasma velocity is given by: $\mathbf{V} = \mathbf{r}_0 d\beta/dt = \mathbf{r}(d\beta/dt)/\beta$. Substituting this expression into Eq. (11.65) and then transforming Euler's variables r, t to Lagrange's ones; that is to r_0, t, we come to

$$\partial_t \mathbf{B} + 2\mathbf{B}\frac{\dot{\beta}}{\beta} = \frac{1}{\mu_0 \sigma_p \beta^2}\nabla^2_{\mathbf{r}_0}\mathbf{B}, \qquad \nabla_{\mathbf{r}_0}\cdot\mathbf{B} = 0, \tag{11.67}$$

where $\dot{\beta}$ denotes the time-derivative and the subscript $\mathbf{r}_0$ stands for derivatives with respect to Lagrange's variables. For simplicity, we will omit the subscript 0 having in mind that now $\mathbf{r}$ is the Lagrange's variable. We seek for the solution of Eq. (11.67) in the form

$$\mathbf{B} = \cos\theta B_1(r,t)\,\hat{\mathbf{r}} - \sin\theta B_2(r,t)\,\hat{\boldsymbol{\theta}}. \tag{11.68}$$

Substituting the Eq. (11.68) into Eq. (11.67) we come to the following equations for the unknown functions B_1 and B_2:

$$\begin{gathered}\partial_t B_1 + 2B_1\frac{\dot{\beta}}{\beta} = \frac{1}{\mu_0\sigma_p\beta^2}\left[B_1'' + \frac{2B_1'}{r} - \frac{4(B_1-B_2)}{r^2}\right],\\ \partial_t B_2 + 2B_2\frac{\dot{\beta}}{\beta} = \frac{1}{\mu_0\sigma_p\beta^2}\left[B_2'' + \frac{2B_2'}{r} + \frac{2(B_1-B_2)}{r^2}\right],\\ B_1' + \frac{2}{r}(B_1 - B_2) = 0.\end{gathered} \tag{11.69}$$

Here the primes denote derivatives with respect to r.

Now we turn to new unknown dimensionless functions $f = (B_1 - B_2)/B_0$ and $g = (B_1 + 2B_2)/B_0 - 3$. These functions satisfy the new set of equations

$$\partial_t f + 2f\frac{\dot{\beta}}{\beta} = \frac{1}{\mu_0\sigma_p\beta^2}\left(f'' + \frac{2f'}{r} - \frac{6f}{r^2}\right); \tag{11.70}$$

$$\partial_t g + 2(g+3)\frac{\dot{\beta}}{\beta} = \frac{1}{\mu_0\sigma_p\beta^2}\left(g'' + \frac{2g'}{r}\right); \tag{11.71}$$

$$2f' + g' + 6f/r = 0. \tag{11.72}$$

Suppose at the initial time there is a uniform magnetic field $\mathbf{B}_0$ everywhere. The initial conditions for the functions f and g are as follows then

$$f(r,0) = g(r,0) = 0. \tag{11.73}$$

The normal and tangential components of $\mathbf{B}$ have to be continuous at the ball surface. Considering this requirement and combining Eqs. (11.66) and (11.68) we come to the following boundary conditions:

$$f(R_0,t) = 3\chi/\beta^3, \qquad g(R_0,t) = 0. \tag{11.74}$$

The set of Eqs. (11.70)–(11.72) with initial and boundary conditions (11.73) and (11.74) contains only two unknown function. However, we shall demonstrate that

this set has a single solution. First of all we note that Eq. (11.72) can be solved for f under a requirement that f is finite when $r \to 0$

$$f = -\frac{1}{2r^3}\int_0^r r_1^3 \partial_{r_1} g\,(r_1, t)\, dr_1. \tag{11.75}$$

Now we prove that if g satisfies Eq. (11.71) then the function f given by Eq. (11.75) must satisfy Eq. (11.70). For this purpose we take the operator $\partial_t + 2\dot{\beta}/\beta$ in order to act on Eq. (11.75). Using Eq. (11.71) we find

$$\partial_t f + 2f\frac{\dot{\beta}}{\beta} = -\frac{1}{2\mu_0\sigma_p\beta^2 r^3}\int_0^r r_1^3 \partial_{r_1}\left(g'' + \frac{2g'}{r_1}\right) dr_1. \tag{11.76}$$

Taking the integral several times by parts and applying Eq. (11.75) we can reduce Eq. (11.76) to the form which is identical with Eq. (11.70). If the solution of Eq. (11.71) under requirements by Eqs. (11.73) and (11.74) is found, then substituting this solution; that is the function g, in Eq. (11.75) gives the function f. Thus one can obtain the unique solution of the problem.

We expand this solution into a series

$$g\,(r, t) = \frac{1}{r}\sum_{n=1}^{\infty} \gamma_n\,(t) \sin\frac{\pi n r}{R_0}, \tag{11.77}$$

where the eigenfunctions $\sin\,(\pi n r/R_0)$ form a complete orthogonal system which satisfies the boundary conditions given by Eq. (11.74). The undetermined functions $\gamma_n\,(t)$ can be found by substituting Eq. (11.77) for g into Eq. (11.71). Taking into account the initial conditions given by Eq. (11.73), we obtain

$$\gamma_n\,(t) = \frac{(-1)^n\, 6R_0}{\pi n\beta^2\,(t)}\int_0^t \frac{d\beta^2}{dt'} \exp\left(-\int_{t'}^t \frac{\pi^2 n^2}{\mu_0\sigma_p R_0^2\beta^2} dt''\right) dt'. \tag{11.78}$$

Substituting Eqs. (11.77) and (11.78) for g and γ_n into Eq. (11.75), and performing integration with respect to r, yield

$$f\,(r, t) = -\frac{R_0^2}{2\pi^2 r^3}\sum_{n=1}^{\infty}\frac{\gamma_n\,(t)}{n^2}\left\{\frac{3\pi n r}{R_0}\cos\frac{\pi n r}{R_0} + \left[\left(\frac{\pi n r}{R_0}\right)^2 - 3\right]\sin\frac{\pi n r}{R_0}\right\}. \tag{11.79}$$

Combining Eqs. (11.74) and (11.79), we finally obtain the dimensionless magnetic moment of the plasma ball

$$\chi = -\frac{3\beta(t)}{\pi^2}\sum_{n=1}^{\infty}\frac{1}{n^2}\int_0^t \frac{d\beta^2}{dt'}\exp\left(-\int_{t'}^{t}\frac{\pi^2 n^2}{\mu_0\sigma_p R_0^2\beta^2}dt''\right)dt'. \tag{11.80}$$

Residual Magnetic Field

First of all consider Eq. (11.23) in the region $R_c < r < R_e$. All the values in Eq. (11.23) are independent of azimuthal angle due to the cylindrical symmetry of the problem. This implies that only azimuthal component of the curl is nonzero. Therefore, substituting of Eq. (9.29) for $\Delta\mathbf{J}$ into Eq. (11.23) gives

$$\frac{1}{r}\left[\partial_r\left(rB_\theta\right) - \partial_\theta B_r\right] = -\mu_0 C_m J d_r s_{rr}\sin\theta, \tag{11.81}$$

where B_r and B_θ are the radial and tangential components of magnetic field and d_r denotes derivative with respect to r, that is $d_r s_{rr} = ds_{rr}/dr$. Maxwell equation $\nabla\cdot\mathbf{B} = 0$ can be written in the form

$$\frac{1}{r^2}\partial_r\left(r^2 B_r\right) + \frac{1}{r\sin\theta}\partial_\theta\left(\sin\theta B_\theta\right) = 0. \tag{11.82}$$

We seek for the solution of Eqs. (11.81) and (11.82) in the form $B_r = B_1(r)\cos\theta$ and $B_\theta = B_2(r)\sin\theta$, where $B_1(r)$ and $B_2(r)$ are unknown functions. This yields

$$d_r\left(rB_2\right) + B_1 = -r\mu_0 C_m J d_r s_{rr}, \tag{11.83}$$

and

$$d_r\left(r^2 B_1\right) + 2rB_2 = 0. \tag{11.84}$$

For the inner and outside areas, i.e. at $r < R_c$ and $r > R_e$, the right-hand side of Eq. (11.83) is equal to zero whereas Eq. (11.84) is valid in the whole space. Integrating of Eq. (11.83) over short intervals $(R_c-\varepsilon, R_c+\varepsilon)$ and $(R_e-\varepsilon, R_e+\varepsilon)$, where $\varepsilon \longrightarrow 0$, gives the boundary conditions for tangential component B_2

$$B_2(R_c+0) - B_2(R_c-0) = -\mu_0 C_m J s_{rr}(R_c), \tag{11.85}$$

$$B_2(R_e+0) - B_2(R_e-0) = \mu_0 C_m J s_{rr}(R_e). \tag{11.86}$$

The continuity of normal component of the magnetic induction results in

$$B_1 (R_c - 0) = B_1 (R_c + 0), \quad B_1 (R_e - 0) = B_1 (R_e + 0), \tag{11.87}$$

Eliminating the function B_2 from the set of Eqs. (11.83) and (11.84), we obtain

$$r d_r^2 B_1 + 4 d_r B_1 = 2\mu_0 C_m J d_r s_{rr} \tag{11.88}$$

The general solution of Eq.(11.88) is given by

$$B_1 = \frac{2\mu_0 C_m J}{r^3} \int_{R_c}^{r} \left(r'\right)^2 s_{rr} \left(r'\right) dr' + \frac{c_1}{r^3} + c_2, \tag{11.89}$$

where c_1 and c_2 are arbitrary constants.

At the regions $r < R_c$ and $r > R_e$ the solution of problem should be limited as $r \longrightarrow 0$ and $r \longrightarrow \infty$. So, we obtain that $B_1 = c_3$ if $r < R_c$ and $B_1 = c_4/r^3$ if $r > R_e$ where c_3 and c_4 are the arbitrary constants. These solutions should fit Eq. (11.89) at the boundaries $r = R_c$ and $r = R_e$. Taking into account the boundary conditions given by Eqs. (11.85)–(11.87) one can find the constants $c_1 - c_4$. Whence it follows that $c_1 = c_2 = c_3 = 0$. So the magnetic field is equal to zero in the inner area at $r < R_c$. For the region $R_c < r < R_e$ one can find

$$B_r = \frac{2\mu_0 C_m J \cos\theta}{r^3} \int_{R_c}^{r} r'^2 s_{rr} \left(r'\right) dr', \tag{11.90}$$

$$B_\theta = \mu_0 C_m J \sin\theta \left(\frac{1}{r^3} \int_{R_c}^{r} r'^2 s_{rr} \left(r'\right) dr' - s_{rr} (r) \right). \tag{11.91}$$

Note that these formulas are more correct than that obtained by Surkov (1989) in the framework of simplified approach which leaves out of account the boundary conditions and thereby the contribution of the surface magnetization currents at $r = R_c$ and $r = R_e$.

References

Ablyazov MK, Surkov VV, Chernov AS (1988) Distortion of an external magnetic field by an expanding plasma sphere located in a slightly conductive semispace. J Appl Mech Tech Phys 29(6):778–784

Adushkin VV, Soloviev SP (1988) Low-frequency electric fields in the atmospheric surface layer during underground explosion. Rep USSR Acad Sci (Dokl Akad Nauk SSSR) 299(4):840–844 (in Russian)

Adushkin VV, Soloviev SP, Surkov VV (1990) Electrical field arising during ejection explosion. Combust Explosion Shock Waves 26(4):478–482
Adushkin VV, Soloviev SP (1996) Generation of low-frequency electric fields by explosion crater formation. J Geophys Res 101B:20165–20173
Allison FE (1965) Shock induced polarization in plastics. 1. Theory. J Appl Phys 36:2111–2113
Baker DM, Davies K (1968) Waves in the ionosphere produced by nuclear explosions. J Geophys Res 73:448–450
Baker DM, Cotten DE (1971) Interpretation of high-frequency Doppler observations of waves from nuclear and natural sources. J Geophys Res 76:1803–1810
Barry GH, Griffiths LJ, JC Taenzer (1966) HF radio measurements of high-altitude acoustic wave from a ground-level explosion. J. Geophys. Res 71:4173–4182
Barsukov OM, Skovorodkin YuP (1969) Magnetic observations in the region of Medeo detonation. Proc USSR Acad Sci Phys Earth (Izvestiya Akad Nauk SSSR Fizika Zemli) 5:68–69 (in Russian)
Baum FA, Orlenko LP, Stanyukovich KP, Chelyshev VP, Shekhter BI (1975) Physics of explosion. In: Stanyukovich KP. Nauka, Moscow, 704 pp (in Russian)
Blanc E (1984) Interaction of an acoustic wave of artificial origin with the ionosphere as observed by vertical HF sounding at total reflection levels. Radio Sci 19:653–664
Blanc E (1985) Observations in the upper atmosphere of infrasonic waves from natural or artificial sources: A summary. Ann Geophys. 3:673–688
Breitling WJ, Kupferman RA, Gassmann GJ (1967) Traveling ionospheric disturbances associated with nuclear detonation. J Geophys Res 72:307–315
Broche P (1977) Propagation des ondes acoustico-gravitationnells excitees par des explosions. Ann Geophys 33:281–288
Chadwick P, Cox AD, Hopkins HG (1964) Mechanics of deep underground explosion. Phil Trans Roy Soc Lond A256:235–300
Chalmers JA (1967) Atmospheric electricity, 2nd edn. Pergamon Press, New York
Colvin JD, Mitchell CK, Greig JR, Murphy DP, Pechacek RE, Raleigh M (1987) An empirical study of the nuclear explosion-induced lightning seen on IVY-MIKE. J Geophys Res 92D:5696–5712
Daniels FB, Bauer SJ, Harris AK (1960) Vertically traveling shock waves in the ionosphere. J Geophys Res 65:1848–1850
Danilov AV, Teselkin SF (1984) A structure of shock wave precursor in weakly ionized anisothermic magnetoactive plasma. Phys Plasma (Fizika Plazmy) 10(4):735–740 (in Russian)
Danilov AV, Dovzhenko VA (1987) On the excitation of electromagnetic fields by acoustic pulses entering the ionosphere. Geomagn Aeron (Geomagnetizm i Aeronomiya) 27(5):772–777 (in Russian)
Enstrom JE, Brode HL, Gilmore FR (1972) Shock propagation in exponential atmospheres. R & D Associates, RDATR042DNA, Santa Monica, California
Erzhanov ZhS, Kurskeev AK, Nysanbaev TE, Bushuev AV (1985) Geomagnetic observations during experiment MASSA. Proc USSR Acad Sci Phys Earth (Izvestiya Akad Nauk SSSR Fizika Zemli) 11:80–82 (in Russian)
Galperin YuI, Hayakawa M (1996) On the magnetospheric effects of experimental ground explosions observed from AUREOL-3. J Geomagn Geoelectr 48:1241–1263
Galperin YuI, Hayakawa M (1998) On a possibility of parametric amplifier in the stratosphere-mesosphere suggested by active MASSA experiments with the AUREOL-3 satellite. Earth Planets Space 1:253–258
Gassmann GJ (1963) Electron density profiles of wave-motions in the ionosphere caused by nuclear detonations, AFCRL Research report. Report US Department of Commerce AD626-694, pp 63–440
Gilinsky V (1965) Kompaneet's model for radio emission from a nuclear explosion. Phys Rev 137A(1):50–55
Gilinsky V, Peebls G (1968) The development of a radio signal from a nuclear explosion in the atmosphere. J Geophys Res 73(1):405–414

Gorbachev LP, Glushkov AI, Kotov YuB, Semenova TA, Skryl'nik AA (1999) Geomagn Aeron (Geomagnetizm i Aeronomiya), Estimate of camouflet explosion power using initial stage of geomagnetic perturbations 39(5):77–82 (in Russian)

Gorbachev LP, Kotov YuB, Semenova TA (1999) Generation of geomagnetic perturbations at late stage of camouflet explosion. Appl Mech Tech Phys (Prikladnaya Mekhanika i Tekhnicheskaya Fizika) 40(4):16–24 (in Russian)

Gorbachev LP, Semenova TA (2000a) Generation of geomagnetic perturbations caused by nuclear underground explosions under decoupling. Pt. 1. Mechanisms of generation. Eng Phys (Inzhenernaya Fizika) 2:66–72 (in Russian)

Gorbachev LP, Semenova TA (2000b) Generation of geomagnetic perturbations caused by nuclear underground explosions under decoupling. Pt. 2. Explosions in evaporated chambers filled by water vapors. Eng Phys (Inzhenernaya Fizika) 4:84–88 (in Russian)

Greifinger C, Greifinger P (1965) Transmission of micropulsations through the lower ionosphere. J Geophys Res 70:2217–2231

Grigor'iev VG, Nemirov AS, Sirotkin VK (1979) Structure of shock waves in elastic-plastic relaxation media. Appl Mech Tech Phys (Prikladnaya Mekhanika i Tekhnitseskaya Fizika) 1:153–160 (in Russian)

Grover MK (1981) Some analytical model for quasi-static source region EMP: Application to nuclear lightning. IEEE Trans Nucl Sci NS-28(1):990–994

Hasbrouk WP, Allen JH (1972) Quasi-static magnetic field changes associated with CANNIKIN nuclear explosions. Bull Seism Soc Am 62(6):1479–1480

Herbst RF, Werth GC, Springer DL (1961) Use of large cavities to reduce seismic waves from underground explosions. J Geophys Res 66(3):959–978

Hill RD (1973) Lightning induced by nuclear bursts. J Geophys Res 78:6355–6358

Holzer RE (1972) Atmospheric electrical effects of nuclear explosions. J Geophys Res 77:5845–5855

Hoppel WA (1967) Theory of electrode effect. J Atmosph Terr Phys 29:709–721

Ivanov KG (1961) Geomagnetic phenomena observed at Irkutsk magnetic observatory after detonation of Tunguska meteorite. Meteoritics 21:46–48 (in Russian)

Jacobson AR, Carlos RC, Blanc E (1988) Observation of ionospheric disturbances following a 5 kt chemical explosion. 1. Persistent oscillation in the lower thermosphere after shock passage. Radio Sci 23:820–830

Johnson MH, Lippman BA (1960) Electromagnetic signals from nuclear explosions in outer space. Phys Rev Ser II 119(3):827–828

Kanellakos DP, Nelson RA (1972) Comparison of computed and observed shock behavior from multikiloton near surface nuclear explosions. Effects of atmospheric acoustic gravity waves on electromagnetic wave propagation. AGARD Confer Proc CP 115(19):240–251

Karlov VD, Kozlov SI, Tkachev GN (1980) Large-scale perturbations in the ionosphere generated by rocket with engine-on flight. A review. Cosmic Res (Kosmicheskie issledovaniya) 18(2):266–277 (in Russian)

Karzas WJ, Latter R (1962a) The electromagnetic signal due to the interaction of nuclear explosions with Earth's magnetic field. J Geophys Res 67(12):4635–4640

Karzas WJ, Latter R (1962b) Electromagnetic radiation from nuclear explosions in space. Phys Rev 126(6):1919–1926

Karzas WJ, Latter R (1965) Detection of the electromagnetic radiation from nuclear explosions in space. Phys Rev 137B(5):1369–1378

Kompaneets AS (1958) Radioemission of atomic explosion. J Exp Theor Phys (Zhurnal eksperimental'noy i teoreticheskoy fiziki) 35(6)(12):1538–1544 (in Russian)

Kompaneets AS (1977) Radio-emission of atomic detonation. II. Physicochemical and relativistic gas dynamics, Selected papers, Nauka, Moscow, pp 83–91 (in Russian)

Kotadia KN (1967) Ionospheric effects of nuclear explosions. Ann Geophys 23:1–11

Landau LD, Lifshitz EM (1959) Fluid mechanics, Vol 6 of A course of theoretical physics. Pergamon Press, New York

Latter AL, LeLevier RE, Martinelly EA, McMillan WG (1961a) A method of concealing underground nuclear explosion. J Geophys Res 66(3):943–946

Latter R, Herbst RF, Watson KM (1961b) Detection of nuclear explosions. Ann Rev Nucl Sci 11:371–375

Lawrie JA, Gerard VB, Gill PJ (1961) Magnetic effects resulting from the Johnston Island high altitude nuclear explosions. N Z J Geology Geophys 4(2):109–124

Leypunskiy OI (1960) On possible magnetic effect under high-altitude detonations of atomic bombs. J Exp Theor Phys (Zhurnal eksperimental'noy i teoreticheskoy fiziki) 38(1):302–304 (in Russian)

Lifshitz EM, Pitaevskii LP (1981) Physical kinetics, course of theoretical physics, Vol 10, Tranls. by J. B. Sykes and R. N. Franklin, Oxford

Lomax JB, Nielson DL (1972) Nuclear weapon effects on the ionosphere (F-region disturbances). Effects of atmospheric acoustic gravity waves on electromagnetic wave propagation. AGARD Confer Proc CP 115(38):495–506

Malik J, Fitzhugh R, Hormuth F (1985) Electromagnetic signals from underground nuclear explosions. Report LA-10545-MS. Los Alamos Natl. Lab., Los Alamos, New Mexico

Marcos FA (1966) Aircraft induced ionospheric disturbances, Sci. Rep. Airforce Surveys in Geophys, vol 175, AFCRL-66-229, Bedford Massachusetts

Medvedev YuA, Stepanov BM, Fedorovich GV (1970) Electric field excited by gamma-quantum pulse in air. J Appl Mech Tech Phys (Zhurnal Prikladnoi Mekhaniki i Tekhnicheskoi Fiziki) 4:3–8 (in Russian)

Medvedev YuA, Fedorovich GV (1975) On the question about radiation of electromagnetic pulses. J Tech Phys (Zhurnal Tekhnicheskoi fiziki) 45(4):697–704 (in Russian)

Medvedev YuA, Stepanov BM, Fedorovich GV (1980) Physics of radiative excitation of electromagnetic fields. Atomizdat, Moscow, 104 pp (in Russian)

Molchanov OA, Hayakawa M (2008) Seismo-electromagnetics and related phenomena: history and latest results. TERRAPUB, Tokyo, 189 pp

Najita K, Huang YN, Fang GTN (1975) Ionospheric disturbances detected over Hawaii after the 1968 French thermonuclear explosion. Ann Geophys 31:301–310

Orlov VV, Uralov AM (1984) The response of the atmosphere to weak surface explosion. Proc USSR Acad Sci Phys Atmos Ocean (Izvestiya Akademii Nauk SSSR, Fizika Atmosfery i Okeana) 6:476–483 (in Russian)

Patterson D (1966) Nuclear decoupling, full and partial. J Geophys Res 71:3427–3436

Pokhotelov OA, Pilipenko VA, Fedorov EN, Stenflo L, Shukla PK (1994) Induced electromagnetic turbulence in the ionosphere and the magnetosphere. Phys Scripta 50:600–605

Pokhotelov O, Parrot M, Fedorov E, Pilipenko V, Surkov V, Gladychev V (1995) Acoustic response of the ionosphere to natural and man-made sources. In: Console R, Nikolaev A (eds) Earthquakes induced by underground nuclear explosions (environmental and ecological problems). NATO ASI series 2/4, Springer, New York, pp 267–279

Rao GL (1972) Ionospheric disturbances caused by long period sound waves generated by Saturn-Apollo launches. Effects of atmospheric acoustic gravity waves on electromagnetic wave propagation. AGARD Confer Proc CP 115(26):329–337

Rodionov VN, Adushkin VV, Kostyuchenko VN, Nikolaevskiy VN, Romashev AN, Tsvetkov VM (1971) In: Sadovsky MA (ed) Mechanical effect of underground explosion. Nedra, Moscow (in Russian)

Sandmeier HA, Dupree SA, Hansen GE (1972) Electromagnetic pulse and time-dependent escape of neutrons and gamma rays from a nuclear explosion. Nucl Sci Eng 48(3):343–352

Semenov AS (1974) Electrical survey based on natural electric field. Nedra, Moscow, 200 pp (in Russian)

Soloviev SP, Surkov VV (1994) Electric perturbations in the atmospheric surface layer caused by an aerial shock wave. Combust Explosion Shock Waves 30(1):117–121

Soloviev SP, Surkov VV (2000) Electrostatic field and lightning generated in the gaseous dust cloud of explosive products. Geomagn Aeron 40(1):61–69

Soloviev SP, Surkov VV, Sweeney JJ (2002) Quadrupolar electromagnetic field from detonation of high explosive charges on the ground surface. J Geophys Res 107(B6):2119
Sorokin VM (2007) Plasma and electromagnetic effects in the ionosphere related to the dynamics of charged aerosols in the lower atmosphere. Russ J Phys Chem B 1(2):138–170
Stacey FD (1964) The seismomagnetic effect. Pure Appl Geophys 58:5–23
Stoffregen W (1962) Ionospheric effects observed in connection with nuclear explosions at Novaja Semlja on 23 and 30 October 1961, FOA3-Rept. A517. Res. Inst. Natl. defense electron. Dept., Stockholm, Sweden
Stoffregen W (1972) Traveling ionospheric disturbances initiated by low-altitude nuclear explosions. Effects of atmospheric acoustic gravity waves on electromagnetic wave propagation. AGARD Confer Proc CP 115(35):471–479
Straker EA (1971) The effect of the ground on the steady-state and time-dependent transport of neutrons and secondary gamma rays in the atmosphere. Nucl Sci Eng 46(3):334–355
Surkov VV (1986) Electromagnetic field produced by a shock wave propagating in a condensed medium. J Appl Mech Tech Phys 27(1):25–31
Surkov VV (1989) Local variations of geomagnetic and geoelectric fields caused by near-surface deformations. Izvestiya Acad Sci USSR Phys Solid Earth 25(5):421–424
Surkov VV (1990a) The propagation of geomagnetic pulsations in the E layer of the ionosphere. Geomagn Aeron 30(1):94–98
Surkov VV (1990b) Propagation characteristics of low-frequency electromagnetic signals due to disturbances in the E layer. Geomagn Aeron 30(5):682–686
Surkov VV (1992a) Excitation of low-frequency geomagnetic oscillations upon the propagation of a vertical acoustic wave in the E layer of the ionosphere. Geomagn Aeron 32(3):332–336
Surkov VV (1992b) Dispersion equations of low-frequency geomagnetic disturbances in the E-layer. Radiophys Quantum Electron 35(9–10):477–486
Surkov VV (1996) Front structure of the Alfvén wave radiated into the magnetosphere due to excitation of the ionospheric E layer. J Geophys Res 101(A7):15403–15409
Surkov VV (2000) Electromagnetic effects caused by earthquakes and explosions, MEPhI, Moscow, 448 pp (in Russian)
Surkov VV, Galperin YuI (2000) Electromagnetic impulse in magnetosphere resulted from impulse of electric current near lower boundary of ionosphere. Cosmic Investig 38(6):602–613
Sweeney JJ (1989) An investigation of the usefulness of extremely low-frequency electromagnetic measurements for treaty verification. Report UCRL-53899, Lawrence Livermore Natl. Lab., Livermore, CA
Sweeney JJ (1995) Low-frequency electromagnetic signals from underground explosions on site inspection: research progress report. Report UCRL-ID-122067. Lawrence Livermore Natl. Lab., Livermore, CA
Sweeney JJ (1996) Low-frequency electromagnetic measurements as a zero-time discriminant of nuclear and chemical explosions – OSI research final report. Report UCRL-ID-126780. Lawrence Livermore Natl. Lab., Livermore, CA
Troitskaya VA (1960) Effects of terrestrial currents caused by high-altitude atomic explosions. Proc USSR Acad Sci Ser Geophys (Izvestiya Akad Nauk SSSR Seriya Geofiziki) 9:1321–1327 (in Russian)
Uman MA, Seacord DF, Price GH, Pierce ET (1972) Lightning induced by thermonuclear detonations. J Geophys Res 77:1591–1596
Undzenkov BA, Shapiro VA (1967) Seismomagnetic effect at magnetite deposit. Proc USSR Acad Sci Phys Earth (Izvestiya Akad Nauk SSSR Fizika Zemli) 1:121–126 (in Russian)
Wåhlin L (1986) Atmospheric electrostatics. Research Studies Press, Wiley, New York, Chichester, Toronto, Brishbane, Singapore, 130 pp
Wait JR (1961) The electromagnetic fields of a horizontal dipole in the presence of a conducting half-space. Can J Phys 39(7):1017–1028
Wait JR (1970) Electromagnetic waves in stratified media, 2nd edn. Pergamon Press, Oxford

Wickersham AF (1970) Detection and analysis of propagating ion-acoustic waves in ionosphere. In: Davies K (ed) Phase and frequency instabilities in electromagnetic wave propagation, AGARD Confer Proc, vol 33. The Advisory Group for Aerospace Research and Development of NATO, pp 421–437

Williams ER, Cooke CM, Wright KA (1988) The role of electric space charge in nuclear lightning. J Geophys Res 93D:1679–1688

Whitham GB (1974) Linear and nonlinear waves. Wiley, New York

Zablocki CJ (1966) Electrical transient observed during underground nuclear explosions. J Geophys Res 71:3523–3542

Zeldovich YaB, Raizer YuP (1963) Physics of shock waves and high-temperature hydrodynamical phenomena. Fizmatgiz, Moscow, 632 pp (in Russian)